Universidad del País Vasco Euskal Herriko Unibertsitatea
VITORIA-GASTEIZKO INGENIARITZA ESKOLA
ESCUELA DE INGENIERÍA DE VITORIA-GASTEIZ

DEGREE IN AUTOMOTIVE ENGINEERING

FINAL DEGREE PROJECT

COMPUTATIONAL MODELLING OF DIFFERENT ELECTRODE CONFIGURATIONS FOR VANADIUM FLOW BATTERIES AT DIFFERENT PRESSURE CONDITIONS

Student: Martínez, López, Joseba

Director (1): Fernández, Gámiz, Unai

Director (2): Aramendia, Iradi, Iñigo

Academic year: 2021-2022

Date: Vitoria-Gasteiz, 17, june, 2022

Universidad del País Vasco Euskal Herriko Unibertsitatea
VITORIA-GASTEIZKO INGENIARITZA ESKOLA
ESCUELA DE INGENIERÍA DE VITORIA-GASTEIZ

GRADO EN INGENIERÍA EN AUTOMOCIÓN

TRABAJO FIN DE GRADO

MODELIZACIÓN COMPUTACIONAL DE DIFERENTES CONFIGURACIONES DE ELECTRODOS PARA BATERÍAS DE FLUJO DE VANADIO A DIFERENTES CONDICIONES DE PRESIÓN

Alumno/Alumna: Martínez, López, Joseba

Director/Directora (1): Fernández, Gámiz, Unai

Director/Directora (2): Aramendia, Iradi, Iñigo

Curso: 2021-2022

Fecha: Vitoria-Gasteiz, 17, junio, 2022

RESUMEN

Mediante este documento se pretende realizar un análisis fluidodinámico de la caída de presión del electrolito de una batería de flujo redox. En el análisis se emplearán programas de CFD (Dinámica de Fluidos Computacional), con el fin de validar los resultados del modelo numérico con los resultados experimentales.

Una vez validado el modelo, se realizarán diferentes diseños tanto de la propia batería como del electrodo mediante herramientas CAD. Estas nuevas geometrías serán analizadas en el programa CFD, de tal forma que se pueda analizar y optimizar el modelo desde el punto de vista fluidodinámico.

ABSTRACT

The aim of this paper is to perform a fluid dynamic analysis of the electrolyte pressure drop of a redox flow battery. CFD (Computational Fluid Dynamics) programs will be used in the analysis in order to validate the results of the numerical model with the experimental results.

Once the model has been validated, different designs of both the battery itself and the electrode will be made using CAD tools. These new geometries will be analysed in the CFD programme, so that the model can be analysed and optimised from the fluid dynamic point of view.

LABURPENA

Dokumentu honen bidez, erredox fluxu-bateria baten elektrolitoaren presio-erorketaren analisi fluidodinamikoa egin nahi da. Analisian CFD (Fluido Konputazionalen Dinamika) programak erabiliko dira, zenbakizko ereduaren emaitzak emaitza esperimentalekin baliozkotzeko.

Eredua baliozkotu ondoren, bateriaren beraren eta elektrodoaren diseinuak egingo dira CAD tresnen bidez. Geometria berri horiek CFD programan aztertuko dira, eredua fluidodinamikaren ikuspegitik aztertu eta optimizatu ahal izateko.

Table of Contents

List of Figures

List of Tables

List of Equations

1. INTRODUCTION

The aim of this Final Degree Project is to carry out a study of the electrolyte flow through the porous media that make up a battery. To this end, Computer Aided Design (CAD) programmes will be used to model the geometries and computational fluid dynamics (CFD) codes will be used to solve the fluid dynamic part of the problem.

In order to put the reader in context, the current situation of the development of energy storage systems will be presented in the State of the Art section. Subsequently, the theoretical basis of fluid dynamics and its application in CFD software, especially for porous media, will be defined.

Next, the necessary geometries will be modelled using CAD programmes. These geometries will then be imported into CFD software, with the aim of comparing these results with the experimental ones, in order to validate the numerical model.

Once the model has been validated, modifications will be made to the geometry in order to identify the most influential parameters and optimise the model.

2. STATE OF THE ART

In recent years, certain factors such as increased demand and concern for the environment have led to an energy transition away from fossil fuels towards renewable energy generation and large-scale energy storage systems[1], [2]. According to Eurostat data, in 2019, nearly 18% of the energy consumed in this territory was of renewable origin[3], very close to the 20% target for 2020. By 2030, the target is set at 32%.

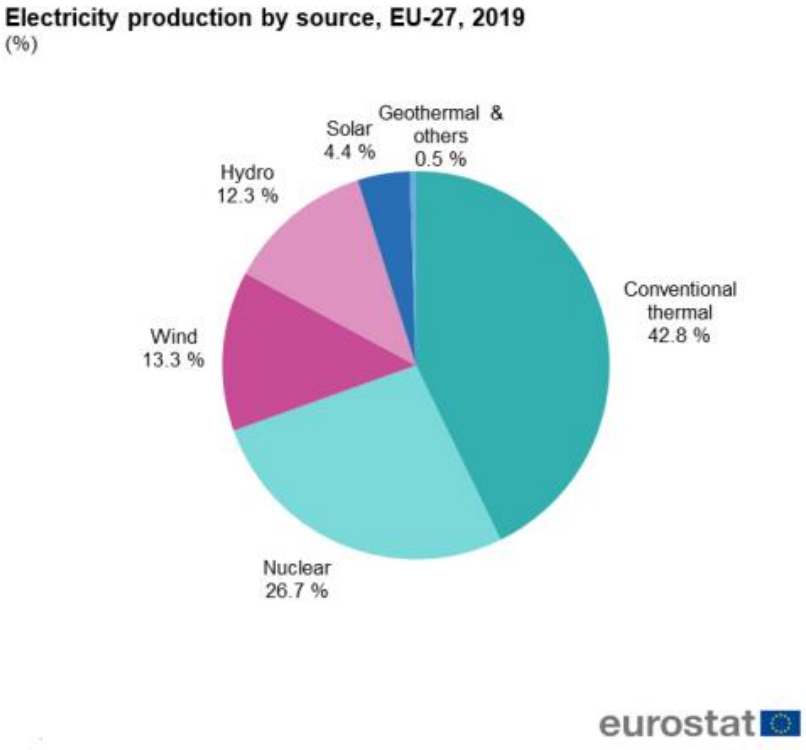

Figure 1. Electricity production by source. Source: eurostat.

However, the world is in constant development, which means a constant increase in power demand. This issue derives in the depletion of natural resources, enviromental and health impact[4]… Over the last years, Energy Storage Systems (ESS) have been the focus of attention, mainly due to the intermittent nature of renewable energy generation[5].

Energy Storage Systems appear as a great option to take fully advantage of renewable energy sources, storing electrical energy to use it when it is really needed. Indeed, the development and implementation of ESS is a serious challenge, as it is still an emerging technology. The main concern comes from reducing costs, improving the efficiency and increasing the capacity[6], [7].

2.1. BENEFITS OF ESS

The installation of ESS offer numerous advantages[8]–[11]:

- Renewable energy integration

As said before, renewebale sources such as solar and wind are random and intermittent, making it difficult for continuos energy production. ESS are able to maximize these assets by storaging energy during off-hours and introudicing it in the grid in peak demand time.

- Load shifting

Thanks to ESS, this new technique has been introduced strategically to reduce energy spending. By analyzing consumption patterns and storage efficiency, special algorythms determine when to charge and discharge the estored energy.

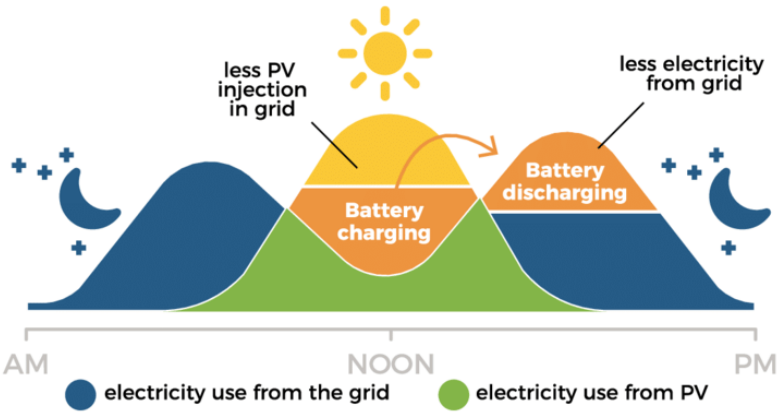

Figure 2. Load shifting strategy.

- Power factor correction

Appart from providing energy during peak demand, Energy Storage Systems can be useful for mitigating low power factors, mantaining the power factor at a desired level.

- Enviromental benefits

Aside from helping integrate renewable energy sources, it can also be useful to reach sustainability goals. For instance, it has no emissions, making it easy to install anywhere. On the other hand, it does help to improve the efficiency of the grid.

2.2. VANADIUM REDOX FLOW BATTERIES (VRFB)

In this context, redox flow batteries (RFB) are an option to be taken into account, which have been the subject of research because of their advantages such as independent control of power and energy. In particular, vanadium redox flow batteries, which were first presented in 1985 by Skyllas-Kazacos[12], are shown to be one of the best alternatives because of their ease of operation and the use of the same electrolyte for both the positive and negative sides of the cell. Their main advantages are shown below[13], [14]:

- Unlike other batteries, power (through stack size) and energy (through tank size) can be controlled independently.
- Low maintenance cost.
- Simplicity and safety of operation.
- Easy scalability and many life cycles.

On the other hand, it has certain disadvantages[15]:

- It is a technology that is still in a consolidation phase.

- The cost of energy storage using this type of battery is still high.
- The energy density is low compared to others such as lithium-ion batteries.
- Low energy and specific power.

Table 1. Comparison of main ESS.

ESS	Max Cycles or Lifetime	Efficiency (%)	Discharge Time	Energy Density (Wh/L)	Capital Cost ($/kW)
Pumped Hydro	30-60 years	70-85	4-12 h	0.2-2	165
Compressed Air	20-40 years	40-70	2-30 h	2-6	105
Flywheel	20,000-100,000	70-95	Secs-mins	20-80	11,520
Lead-acid battery	6-40 years	80-90	1 min-8 h	50-80	1040
Li-ion battery	1,000-10,000	85-95	1 min-8 h	200-400	1084
Redox Flow Battery	12,000-14,000	60-85	Hours	20-70	2220

The main components of a VRFB are: the electrolyte, which is stored in two separate tanks, two electrodes where the chemical reactions take place and an ion exchange membrane that keeps the two electrodes apart. The main lines of research focus especially on the latter two components.

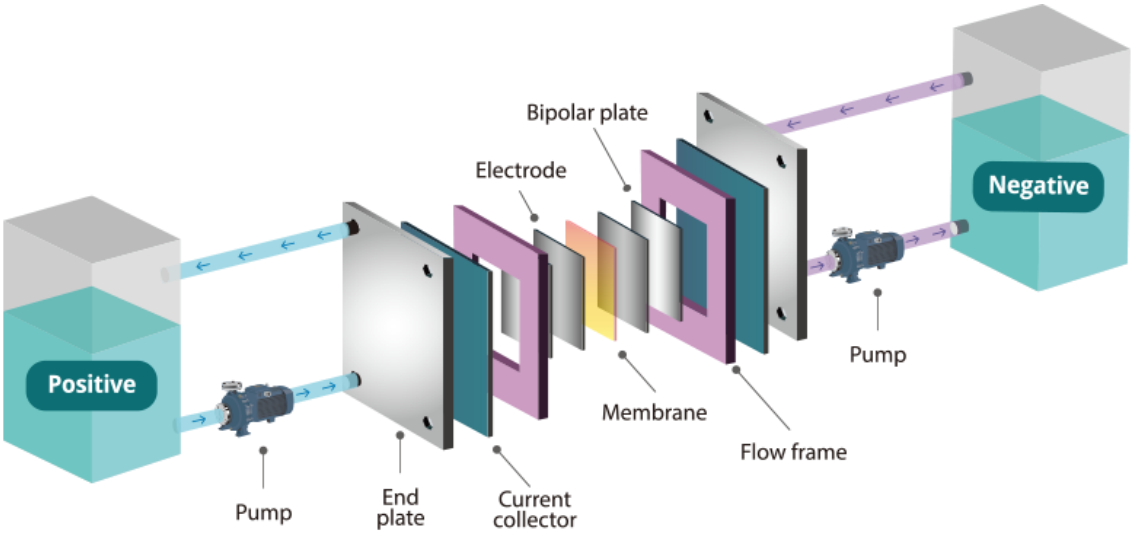

Figure 3. VRFB scheme. Source [16]

2.2.1. WORKING PRINCIPLE

As explained above, the electrolyte is stored in two separate tanks. Each tank contains vanadium in two different oxidation states, V^{2+} and V^{3+} in one, V^{4+} and V^{5+} in the other. By means of mechanical pumps, the electrolyte is pumped across the electrodes, where the chemical reactions take place. The membrane is responsible for preventing cross contamination between the vanadium species on each side, while selectively allowing hydrogen protons to pass through, in order to maintain charge balance. The reactions are shown below:

$$Positive\ cell: VO_2^+ + 2H^+ + e^- \leftrightharpoons VO^{2+} + H_2O \qquad (1)$$

$$Negative\ cell:\ V^{2+} \leftrightharpoons V^{3+} + e^{-} \qquad (2)$$

$$Cell\ reaction:\ VO_2^{+} + V^{2+} + 2H^{+} \leftrightharpoons VO^{2+} + V^{3+} + H_2O \qquad (3)$$

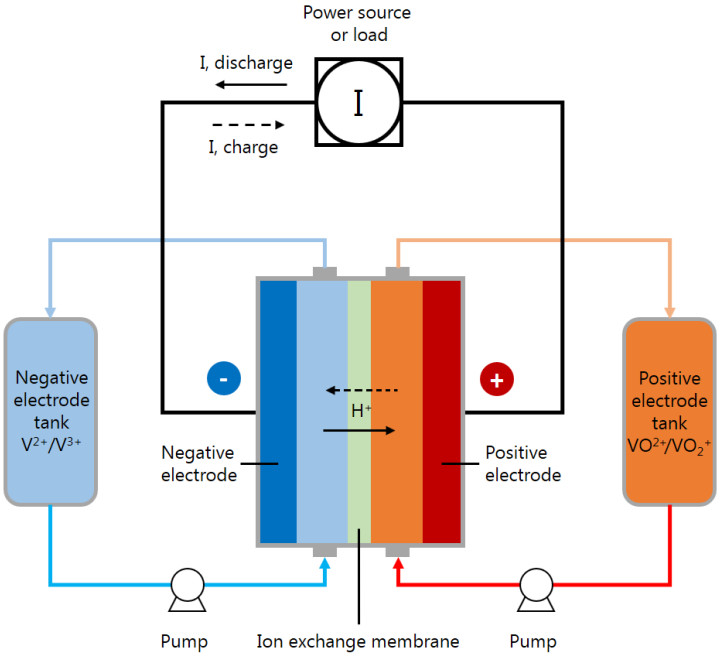

Figure 4. VRFB working scheme.

During charge process at the cathode (positive side), VO^{2+} (V^{4+}) is oxidized to VO_2^{+} (V^{5+}), while at the anode (negative side), V^{2+} is reduced to V^{3+}. The hydrogen protons $2H^{+}$ pass through the membrane to mantain the charge equilibrium.

2.2.2. MAIN COMPONENTS

Electrolyte

It is one of the key components in a VRFB, as the volume of electrolyte determines the capacity of the battery. It is composed of active redox couples and supporting electrolytes. For the redox couples, V(II)/V(III) and V(IV)/V(V) are frequently used, while for the supporting electrolyte, the suplhuric acid has been proven as one of the most suitable options[17].

One of the main concerns about the electrolyte is low the energy density, which restricts its applications. It depends on the electrolyte's composition, usually being limited to 15-25 Wh/kg[18].

Electrode

The electrode is the component which provides the reaction site for the redox couples. Though it does not participate in the reaction, its surface plays as a catalyst, being responsable for

getting/providing electrical current from the cell when discharging/charging and capturing the electrons released in the reaction[17], [18].

The main requirements for the electrode are[19]:

- To remain electrochemically stable during the operation window.
- High electrical conductivity for fast charge transfer reactions.
- Optimal porosity in order to reach the right pressure-drop/reaction-rate equilibrium.
- Highly catalytic material.

Graphite felt (GF) electrodes have been widely researched and used in these last years, thanks to improving cell mixing, reactions and mass transport. However, this type of electrodes have poor wettability. In order to solve this, a pretreatment is usually applied to the surface. Another aspect that has shown promising results is the reduction of the distance between electrodes. In this architecture, known as "zero-gap", the electrodes, current collectors and membrane are in direct contact, thus reducing internal ohmic resistance and voltage drop, and achieving high current densities[20], [21].

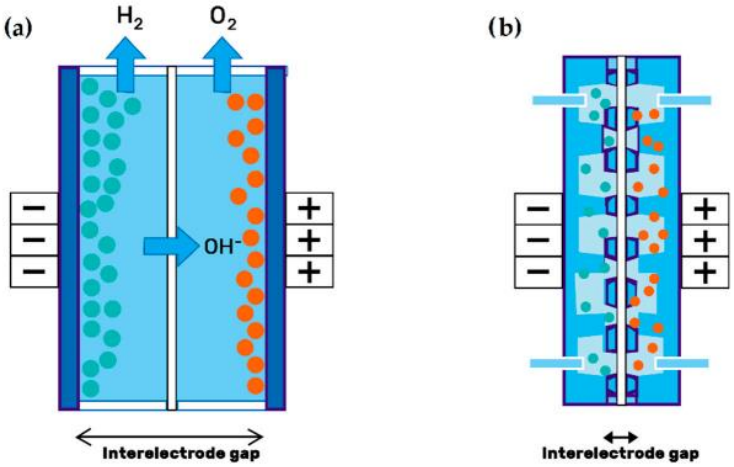

Figure 5. Electrode configuration: (a) Traditional setup; (b): zero-gap design of porous electrodes. Source [22].

There are two electrode configurations for the flow field: "flow-by" and "flow-through". The "flow-by" configuration was adopted as the best option, due to its better electrolyte distribution through the electrode[23], [24]. This difference is more remarkable at high flow rates, when the "flow-through" configuration exhibits too high pressure drop values.

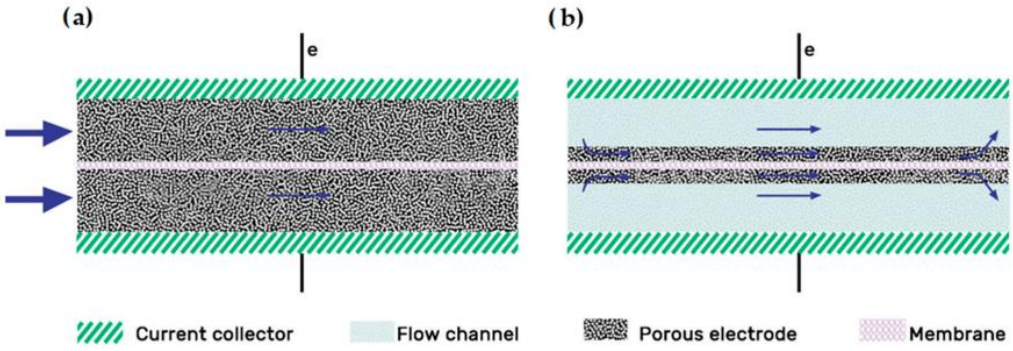

Figure 6. Electrode designs: (a) Flow-thorugh; (b) Flow-by electrode configurations. Source [22].

Ion Exchange Membrane

The membrane is the component designed to be a separator between the anode and cathode, consequently isolating the active species from each side. It also allows the transport of ions to mantain the charge balance in the cell[17].

The desired characteristics for the membrane are[17]:

- High efficiency over many cycles.
- High ionic conductivity.
- Low vanadium ion permeability.
- Chemical stability in the long term.
- Low cost.

Ion exchange membranes can be classified into anion exchange (AEM) and cation exchange (PEM) membranes. Nowadays, Nafion membranes are the most commonly used for VRRB applications. Their high ionic conductivity and chemical stability make them a great option, although they have a high cost and low coulombic efficiency.

2.3. GENERAL EQUATIONS OF FLUID MECHANICS

In order to give an introduction in the fundamentals of fluid mechanics, the governing equations will be presented in this section[25].

2.3.1. CONTINUITY EQUATION

The continuity equation expresses a mass balance for a flowing volume over time. For an infinitesimal element inside that moving fluid, its shape and volumen willl change, but not its mass. The equation will be, for a non-stationary, three-dimensional system and for a compressible fluid:

$$\frac{\partial \rho}{\partial t} + \nabla \cdot (\rho v) = 0 \qquad (4)$$

Where ρ refers to the fluid's density, t is time and v is fluid's velocity.

2.3.2. MOMENTUM EQUATION

Referring to Newton's Second Law, the sum of the forces acting on a particle is equal to the change in the particle's amount of motion. In this way, the equations for three dimensions are:

$$\rho \frac{\partial v}{\partial t} = -\frac{\partial p}{\partial x} + \frac{\partial \tau_{xx}}{\partial x} + \frac{\partial \tau_{yx}}{\partial y} + \frac{\partial \tau_{zx}}{\partial z} + \rho f_y \qquad (5)$$

$$\rho \frac{\partial v}{\partial t} = -\frac{\partial p}{\partial x} + \frac{\partial \tau_{xy}}{\partial x} + \frac{\partial \tau_{yy}}{\partial y} + \frac{\partial \tau_{zy}}{\partial z} + \rho f_y \qquad (6)$$

$$\rho \frac{\partial v}{\partial t} = -\frac{\partial p}{\partial x} + \frac{\partial \tau_{xz}}{\partial x} + \frac{\partial \tau_{yz}}{\partial y} + \frac{\partial \tau_{zz}}{\partial z} + \rho f_y \qquad (7)$$

Where p refers to the fluid's pressure, τ is the shear stress and ρf_y refers to external forces.

2.3.3. ENERGY EQUATION

This equation is an extension of the First Law of Thermodynamics, which states that the energy variation of a fluid's particle is equal to the particle's heat variation plus the work done on the particle.

$$\begin{Bmatrix} Rate\ of\ change\ of \\ energy\ inside\ the \\ fluid\ element \end{Bmatrix} = \begin{Bmatrix} Net\ flux\ of \\ heat\ into \\ the\ element \end{Bmatrix} + \begin{Bmatrix} Rate\ of\ work\ done\ on \\ the\ element\ due\ to\ body \\ and\ surface\ forces \end{Bmatrix} \qquad (8)$$

or,

$$A = B + C \qquad (9)$$

In this way, each term would result in:

$$A = \rho \frac{\partial}{\partial t}\left(e + \frac{V^2}{2}\right) dx\, dy\, dz \quad (10)$$

$$B = \left[\rho \dot{q} + \frac{\partial}{\partial x}\left(k \frac{\partial T}{\partial x}\right) + \frac{\partial}{\partial y}\left(k \frac{\partial T}{\partial y}\right) + \frac{\partial}{\partial z}\left(k \frac{\partial T}{\partial z}\right)\right] dx\, dy\, dz \quad (11)$$

$$C = -\left[\left(\frac{\partial (up)}{\partial x}\right) + \left(\frac{\partial (vp)}{\partial y}\right) + \left(\frac{\partial (wp)}{\partial z}\right) + \frac{\partial (u\tau_{xx})}{\partial x} + \frac{\partial (u\tau_{yx})}{\partial y} + \frac{\partial (u\tau_{zx})}{\partial z} + \frac{\partial (v\tau_{xy})}{\partial x} + \frac{\partial (v\tau_{yy})}{\partial y} + \frac{\partial (v\tau_{zy})}{\partial z} + \frac{\partial (w\tau_{xz})}{\partial x} + \frac{\partial (w\tau_{yz})}{\partial y} + \frac{\partial (u\tau_{zz})}{\partial z}\right] dx\, dy\, dz + \rho f \cdot V\, dx\, dy\, dz \quad (12)$$

A refers to the sum of the internal and kinetic energy of the particle, while B takes into account the heat net flux in the three directions. C refers to the sum of the work done by the surface and body forces on the three directions.

2.4. POROUS MEDIA MODELLING

Modeling of flows through a porous medium requires a modified formulation of the Navier-Stokes equations, which reduces to their classical form and includes additional resistance terms induced by the porous region.

In this situation, Darcy's Law needs to be applicated. Darcy's Law is a derived constitutive equation that describes flow through a porous region. Darcy's law at constant elevation is a simple proportional relationship between the instantaneous discharge rate through a porous medium, the viscosity of the fluid, and the pressure drop over a given distance.

$$Q = -\frac{kA(p_b - p_a)}{\mu L} \quad (13)$$

The total discharge Q has units of volume per time, for instance m^3/s, is equal to the product of the permeability of the medium, m^2, the cross-sectional area of the flow, A, with units of area, for instance m^2, and the total pressure drop ($p_b - p_a$) (Pa), all divided by the viscosity, μ (Pa), and the length over which the pressure drop is taking place, L. The negative sign is needed because fluid flows from high pressure to low pressure. Dividing both sides of the equation by the area and using more general notation leads to:

$$q = \frac{-k}{\mu} \Delta p \quad (14)$$

where *q* is the flux discharge per unit area, often referred to as Darcy flux,with units of length per time, m/s, and Δ*p* is the pressure gradient vector (Pa/m)[26].

It is important to note that Darcy flux does not equal the fluid velocity, as only a fraction of the total volume is available for flow. The fluid velocity is found through the average linear velocity,

which is average of the velocity of all possible fluid paths through the porous media. Instead, we will note that the fluid velocity is:

$$\boldsymbol{v = \frac{q}{\varphi}} \qquad (15)$$

where φ is the porosity and v is the fluid velocity. The porosity, φ is calculated as ratio of the volume of void space to the the total volume of a material $\varphi = \frac{Vvoid}{Vtot}$ and is usually expressed as a fraction between 0 and 1 or as a percent.

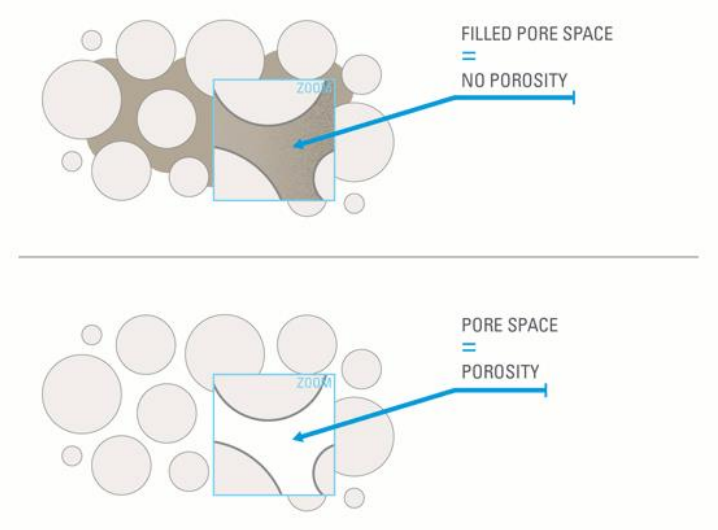

Figure 7. Porosity.

Another term that arises when discussing flow through porous media is permeability. While porosity is the actual fraction of pores (voids), these voids can have different shapes and different connectivity, which affects how easily a fluid can move through the pore space. The permeability is a measure of the ease with which liquids and gases can pass through a porous region. The more consolidated the material, the lower its permeability[27].

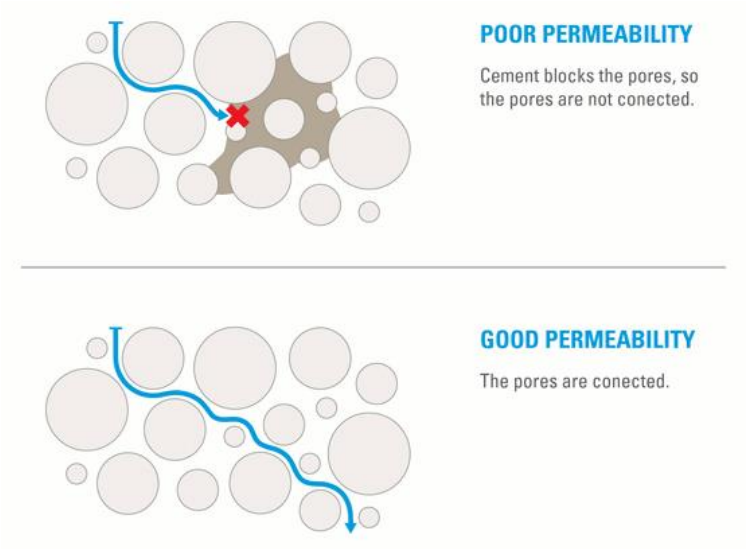

Figure 8. Permeability.

3. METHODOLOGIES

After the literature review, the objective of the project will be presented. In this case the focus will be on the fluid dynamic part of a VRFB.

The objective is to generate a numerical model capable of correctly reflecting the flow behaviour in porous media such as the electrode. First, the generated model needs to be validated. For this purpose, six electrode compressions will be tested in the model: 0, 11, 22, 33, 43 and 54%. In each of these compressions, 10 values of inlet velocities and outlet pressures will be tested, and the results obtained will be compared with the experimental results to validate the model.

After validation, the influence of the dimensions of the electrode itself and the geometry external to it will be analysed.

3.1. MODEL VALIDATION

In order to demonstrate that the numeric model represents accurately the reality, an experimental validation is carried out. In the present case, it has been performed comparing the numerical results with the experimental ones brought out by Tekniker.

The experimental model consisted of a cell, composed by an inlet, outlet and a porous electrode between them, same as the numerical model. Water was pumped through the cell by mechanical pumps, and flow rate, inlet and outlet pressure were measured. The flow rate was altered by changing the pumps RPM, having 10 diffferent RPM for each electrode compression value. This experimental data is summarised in Tables 2, 3 and 4.

Table 2. Flow rate (ml/min).

RPM	% COMPRESION						
	0	11	22	33	43	54	65
70	110	110	110	110	110	104	94
90	122	122	122	126	140	142	130
110	150	150	150	158	170	164	158
130	178	178	182	188	202	194	170
150	208	208	210	219	238	228	182
170	240	240	240	248	272	260	
190	270	270	275	282	318	290	
210	304	306	308	318	338	292	
230	326	330	340	341	374	320	
250	360	368	368	372	408	333	

Table 3. Inlet Pressure (kPa).

Compresion	RPM									
	70	90	110	130	150	170	190	210	230	250
0%	5	6	8	9	11	13	14	17	19	21
11%	8	10	13	15	18	21	24	28	30	33
22%	14	17	22	26	30	34	39	44	49	52
33%	23	29	37	43	49	56	64	72	78	83
43%	37	47	59	67	78	88	99	110	121	127
54%	61	81	98	112	128	144	163	178	194	203
65%	102	137	165	186	212	236	267	287	312	323

Table 4. Outlet Pressure (kPa).

Compresion	RPM									
	70	90	110	130	150	170	190	210	230	250
0%	1.23	1.21	1.16	1.20	1.32	1.37	1.49	1.58	1.71	1.50
11%	0.92	0.93	0.98	1.00	1.11	1.20	1.24	1.56	1.39	1.30
22%	1.16	0.99	1.04	1.12	1.04	1.12	1.30	1.58	1.42	1.50
33%	0.95	0.94	1.00	0.52	1.06	1.12	1.30	1.30	1.42	1.50
43%	1.30	1.20	1.00	1.12	1.14	1.11	1.30	1.30	1.30	1.50
54%	0.89	0.93	0.98	1.12	1.26	1.11	1.30	1.30	1.30	1.50
65%										

Having this data, by performing some calculations, we can get the velocity values we need to introduce in the numerical model.

First, we can calculate the inlet tube area, as we know its diameter:

$$Tube\ area = \frac{\pi \cdot D^2}{4} = \frac{\pi \cdot (5.5 \cdot 10^{-3})^2}{4} = 2.38 \cdot 10^{-5}\ m^2 \qquad (16)$$

So, taking the first value from Table 2, we can convert the flow rate from *ml/min* to m^3/s and consequently, calculate the inlet velocity:

$$Flow\ rate\ conversion: \frac{110\ ml}{min} \cdot \frac{min}{60\ s} \cdot \frac{l}{10^3\ ml} \cdot \frac{m^3}{10^3\ l} = 1.83 \cdot 10^{-6} \frac{m^3}{s} \qquad (17)$$

$$v = \frac{Q}{A} = \frac{1.83 \cdot 10^{-6}\ m^3/s}{2.38 \cdot 10^{-5} m^2} = 0.07716\ m/s \qquad (18)$$

Results after applying this to all values are shown in Table 5.

Table 5. Inlet Velocity (m/s).

RPM	% COMPRESION						
	0	11	22	33	43	54	65
70	0.077166033	0.077166	0.077166	0.077166	0.077166	0.072957	0.065942
90	0.085584146	0.085584	0.085584	0.08839	0.098211	0.099614	0.091196
110	0.105226409	0.105226	0.105226	0.110838	0.119257	0.115048	0.110838
130	0.124868672	0.124869	0.127675	0.131884	0.141705	0.136093	0.119257
150	0.145913953	0.145914	0.147317	0.153631	0.166959	0.159944	0.127675
170	0.168362254	0.168362	0.168362	0.173974	0.190811	0.182392	
190	0.189407536	0.189408	0.192915	0.197826	0.22308	0.203438	
210	0.213258855	0.214662	0.216065	0.22308	0.23711	0.204841	
230	0.228692061	0.231498	0.238513	0.239215	0.262365	0.224483	
250	0.252543381	0.258155	0.258155	0.260961	0.286216	0.233603	

3.1.1. GEOMETRY

The base model design was provided by Tekniker, shown in Figure 9. It consists of a VRFB cell, having both an inlet and outlet channel for the electrolyte, and a porous electrode.

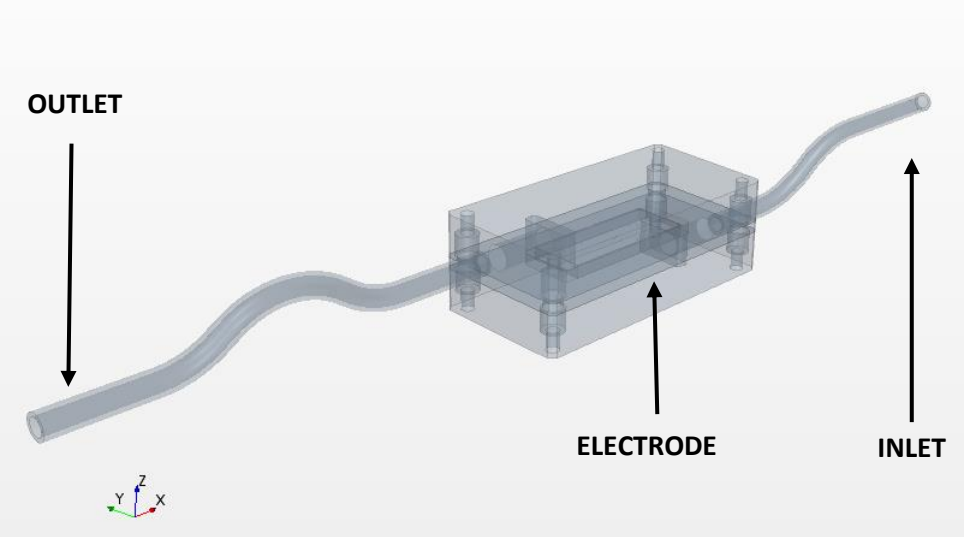

Figure 9. Base model design.

As the analysis will only involve the fluid dynamic part of the battery, the model was simplified and sketched. This was performed using a CAD software, SIEMENS NX 12. Here below battery dimensions and final CAD design can be seen in detail.

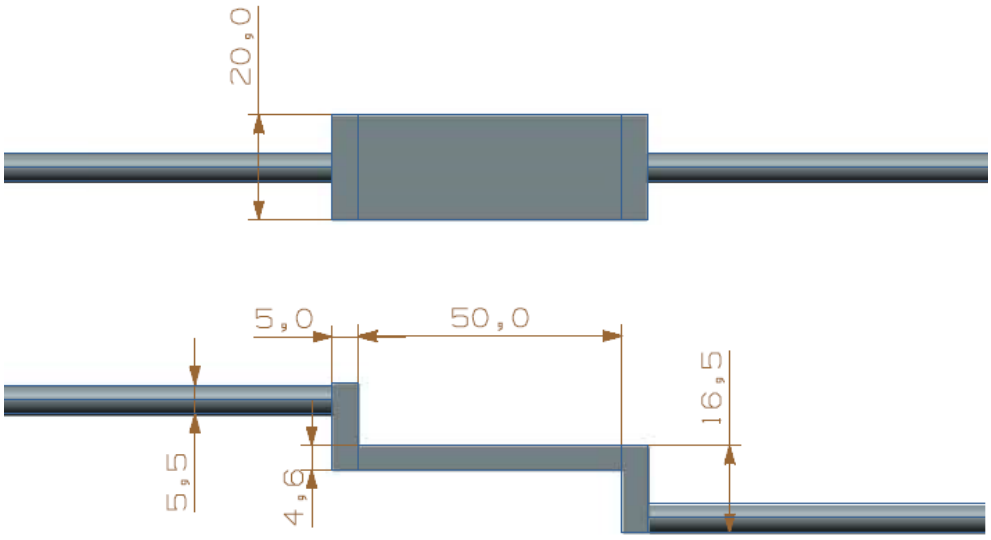

Figure 10. Simplified CAD.

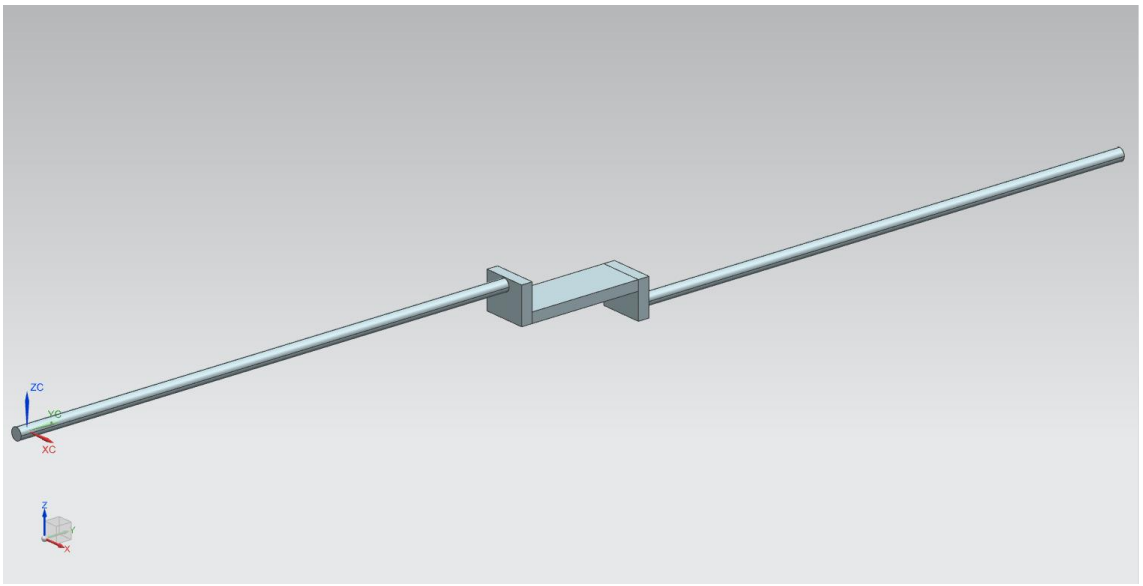

Figure 11. 3D CAD.

3.1.2. CFD

Once the CAD is finished, the file is then imported to the CFD software. In this case *COMSOL Multiphysics* will be used, as it has a proper module for modelling porous media.

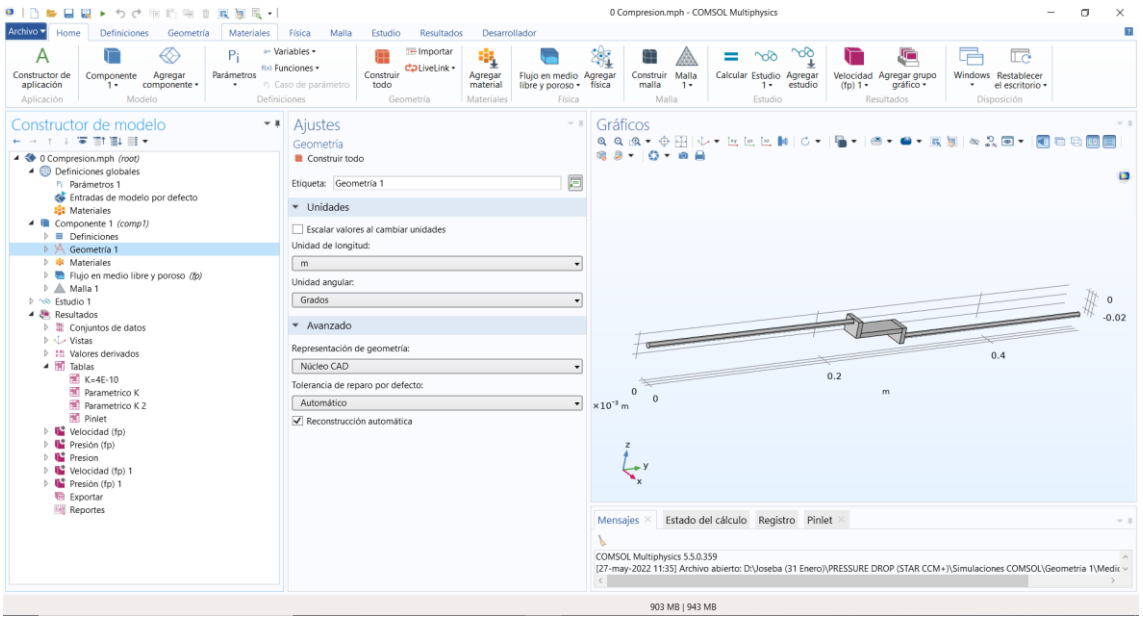

Figure 12. Model imported in COMSOL.

3.1.2.1. PARAMETERS

COMSOL Multiphysics has the possibility to define a list of parameters, in order to make it easier to change values when doing multiple simulations. In this list, we define the electrode's permeability (K) and porosity (por), the inlet velocity and outlet pressure of the system.

As said before, the electrode will be compressed from 0% to 54%, so porosity and permeability values will change. Porosity is calculated using this relation[28]:

$$\varepsilon = 1 - \frac{(1-\varepsilon_0)\cdot t_0}{t_c} \qquad (19)$$

Where t_0 is the original thickness of the electrode, t_c is the thickness of the electrode compressed and ε_0 is the original porosity. From the GFD 4.6 EA manufacturer's data [29] original porosity and thickness are known. After calculating porosity and calibrating permeability for each compression case, results are summarised in Table 6:

Table 6. Electrode's porosity and permeability variation.

Electrode's compression (%)	Porosity (-)	Permeability (m^2)
0	0.94	1.9E-10
11	0.932584	1.16E-10
22	0.923077	0.76E-10
33	0.919448	0.52E-10
43	0.894737	0.43E-10
54	0.869565	0.33E-10

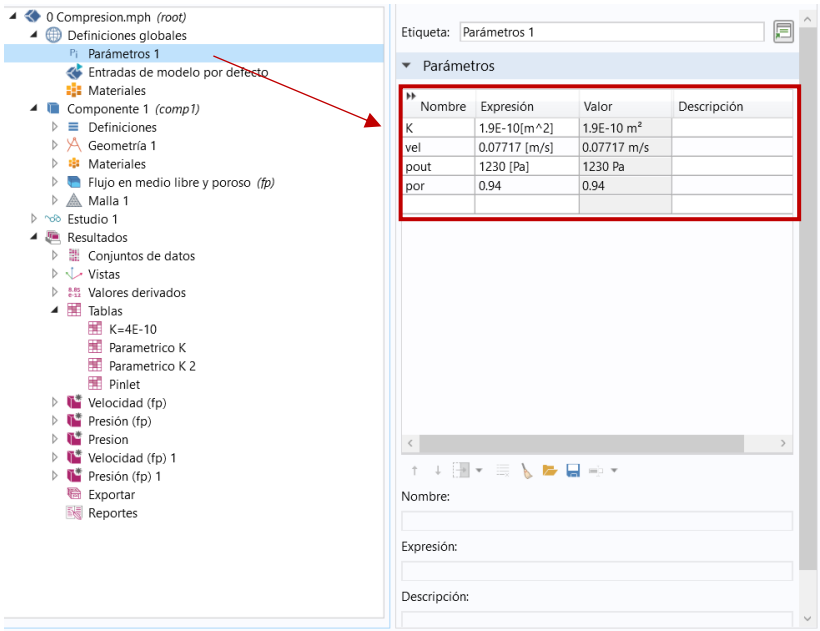

Figure 13. Creation of parameters in COMSOL.

3.1.2.2. PHYSICS AND BOUNDARY CONDITIONS

The Free and Porous Media Flow interface is useful for modeling problems where free flow is connected to porous media[30]. The Free and Porous Media Flow interface is used over at least two different domains, a free channel and a porous medium. In this case, it fits perfectly, as the model consists of a free flow region until it reaches the electrode, and then it goes again through a free flow region.

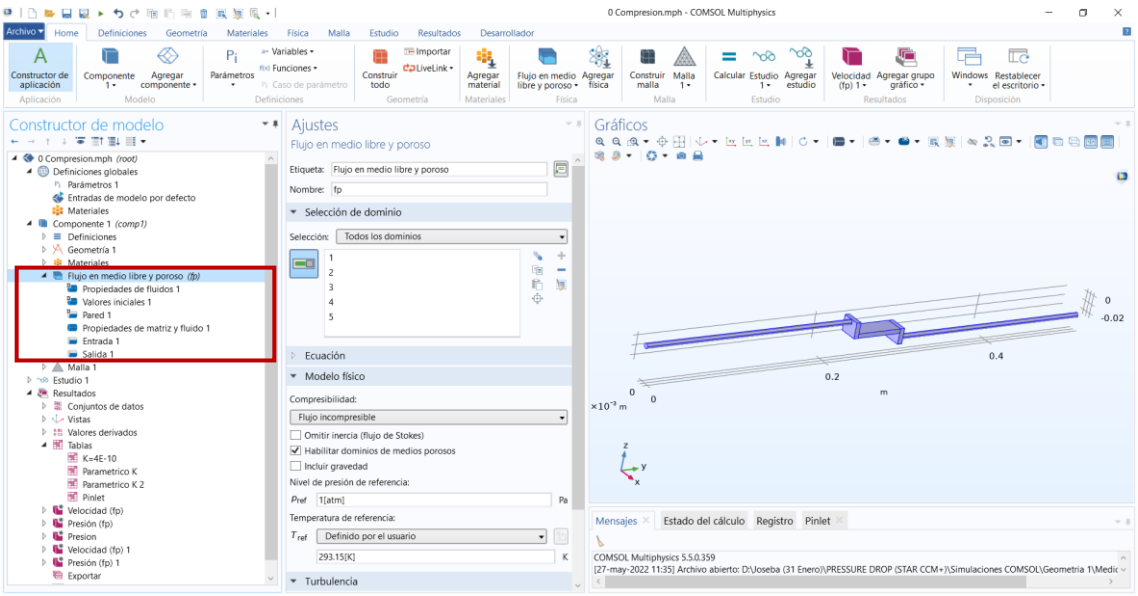

Figure 14. Free and Porous Media Flow Module.

After that, some properties need to be defined (Figure 15):

- Fluid incompressibility
- Reference pressure of 1 atm
- Reference temperatura of 293.15 K
- Laminar flow

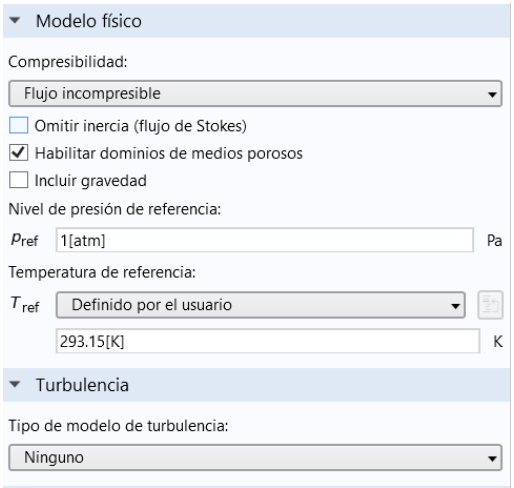

Figure 15. Physical properties.

The first option that comes with Free and Porous Media Flow physics is Fluid Properties. Fluid density and kinematic viscosity are defined here. *COMSOL* has a material library included, so water has been chosen and its properties are automatically applied. The blue highlighted areas

in the geometry, (right part of the image) are the domains where this conditions are going to be applied, in this case everything except for the electrode.

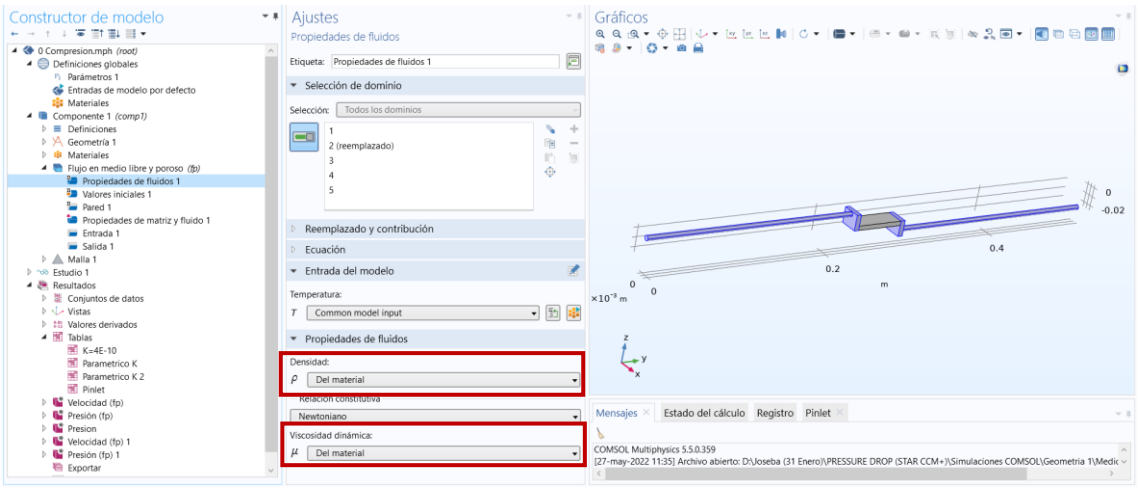

Figure 16. Fluid properties.

After that, another domain called Fluid and Matrix Properties is added to specifiy electrode properties, such as porosity and permeability. This is done in the Porous Matrix Properties section. In this case, we only select the electrode domain (highlighted in blue).

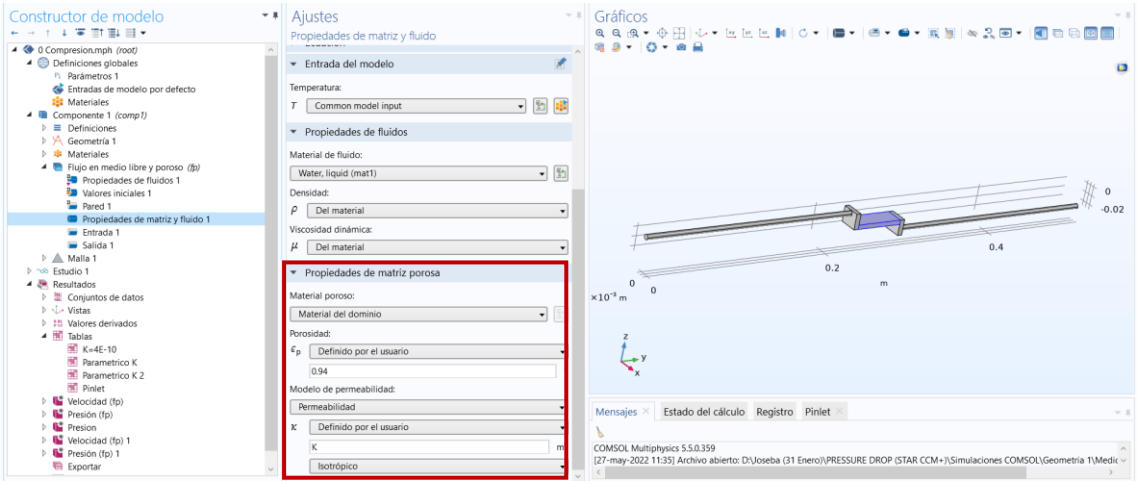

Figure 17. Matrix properties.

Following this, boundary conditions are needed, being the inlet the first. As it can be seen in Figure 18, an Inlet contour has been added, selecting the boundary located in the lower tube. In the Inlet window, “normal inlet speed” option is selected, and the value has been defined by the results shown in Table 5.

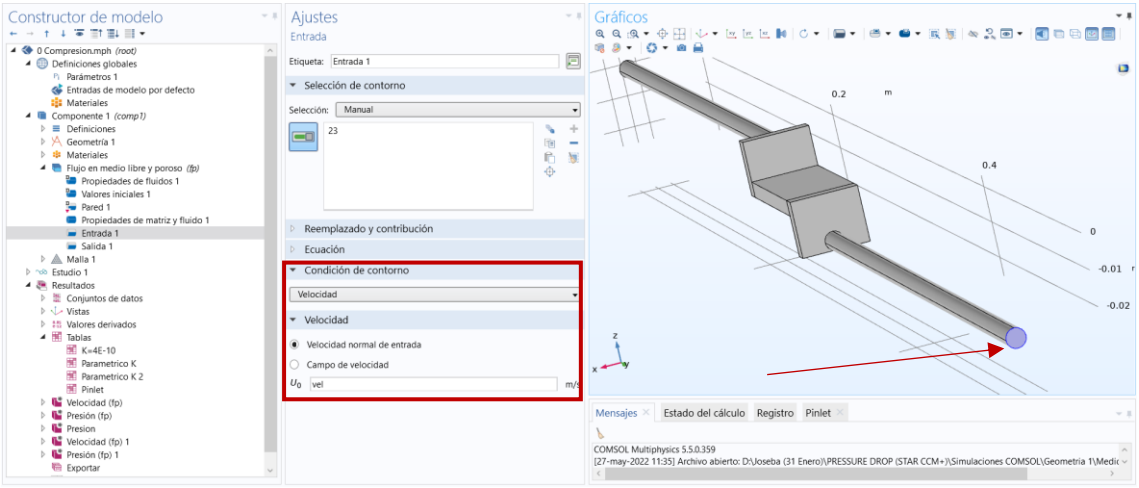

Figure 18. Fluid Inlet.

The same procedure has been done for the fluid outlet. An Outlet contour has been added, and the pressure value is defined also by the parameter created before.

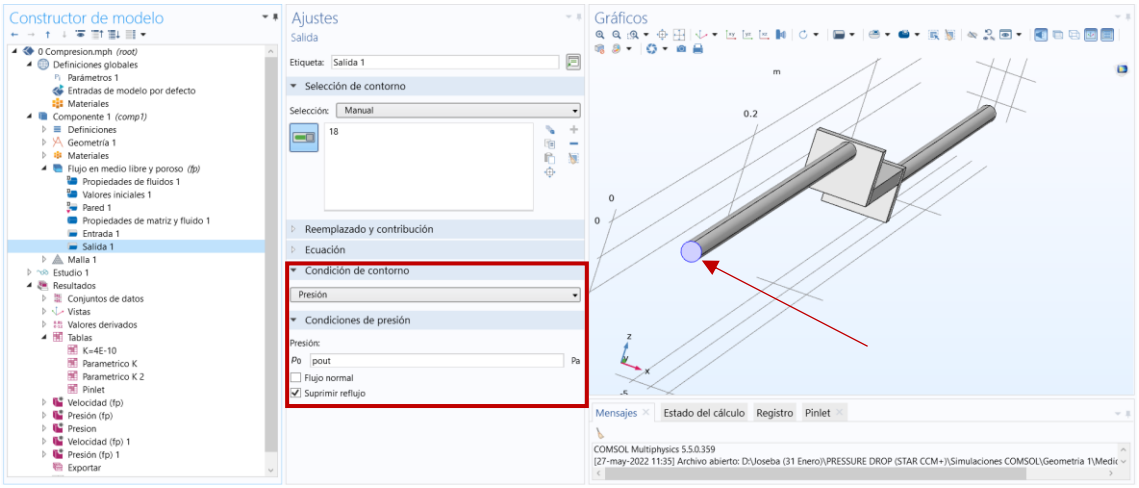

Figure 19. Fluid Outlet.

3.1.2.3. MESH

Once the physics and boundary conditions are applied, the domains need to be discretized by meshing them. *COMSOL* offers different element types for the mesh. For this model, tetraedric elements are chosen. In Size window many configuration options are available to make the mesh suitable. Another aspect to consider is the possibility to calibrate the mesh for a specific kind of physics, as it can be appreciated in Figure 20.

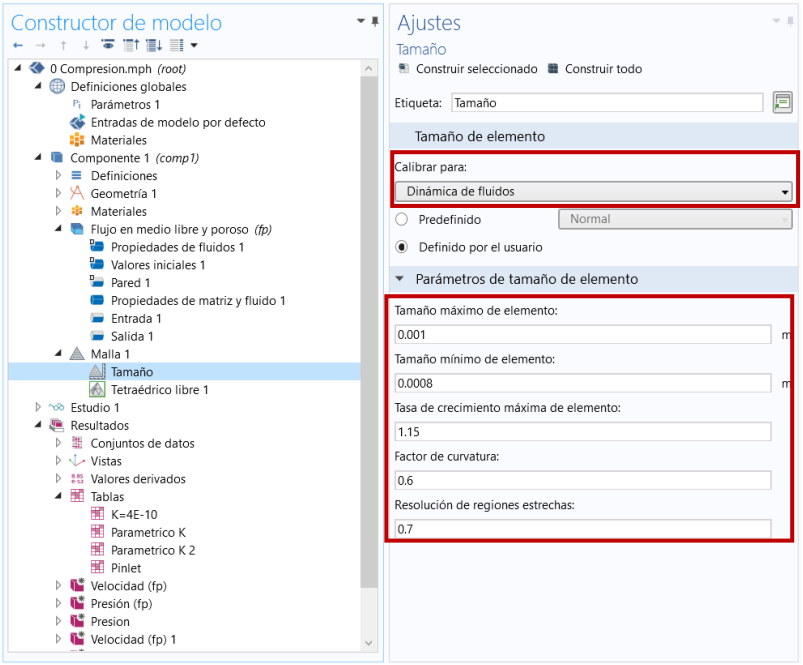

Figure 20. Mesh parameters.

As the compression of the electrode increases, the gradients of the physical quantities will become more pronounced, and therefore the mesh will have to be refined. In Table 7 the elements needed for each compression can be seen.

Table 7. Mesh elements for each compression.

Electrode's compression (%)	Number of elements
0	292405
11	402577
22	843525
33	928775
43	1290017
54	2149851

Below 3 images are shown to appreciate the mesh in detail.

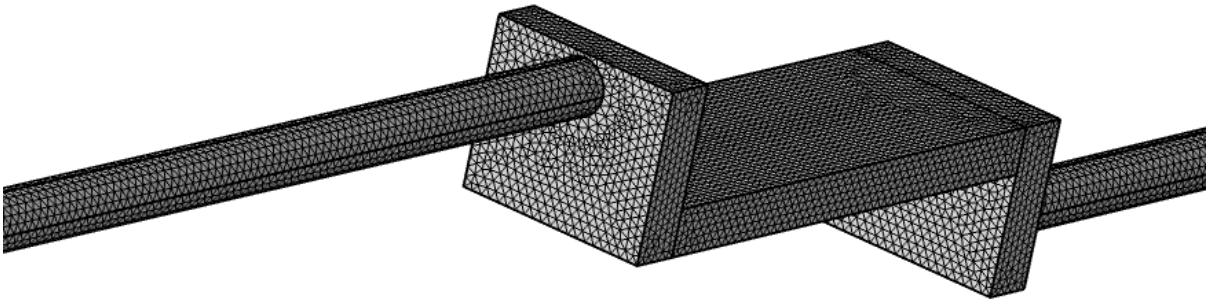

Figure 21. Mesh.

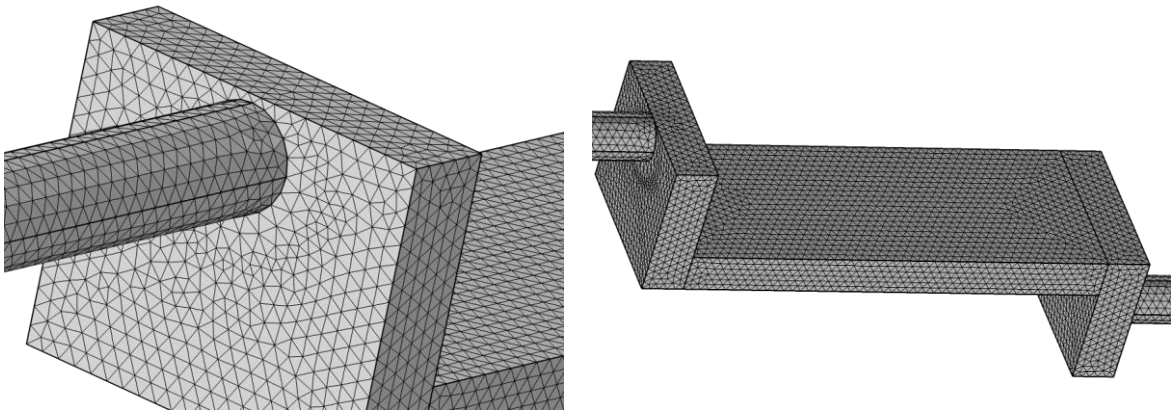

Figure 22. Mesh in detail.

3.1.2.4. SIMULATION CONDITIONS

Before starting to run the simulation, *COMSOL* needs to define the type of *Study* to be performed. In this case, *Stationary* is selected. Due to the numerous cases to run, a *Parametric Sweep* was added to each compression, as each one of them has 10 different values for inlet velocity and outlet pressure.

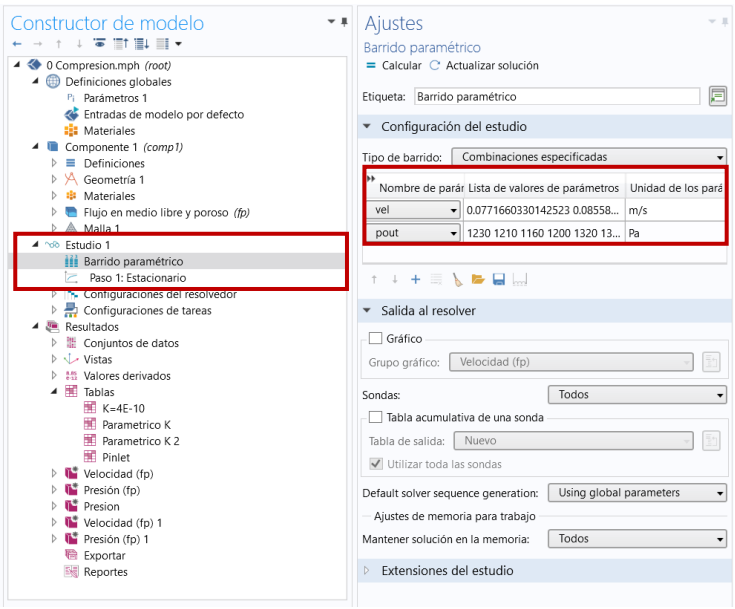

Figure 23. Parametric Sweep.

3.1.3. RESULTS

In this section the numerical results obtained will be compared with the experimental ones. The values of the pressure drop (dP) along the model for each RPM case are shown below.

The graphics show precise agreement between experimental and numerical results. Note that increasing the RPM means an increase in the pressure loss along the battery.

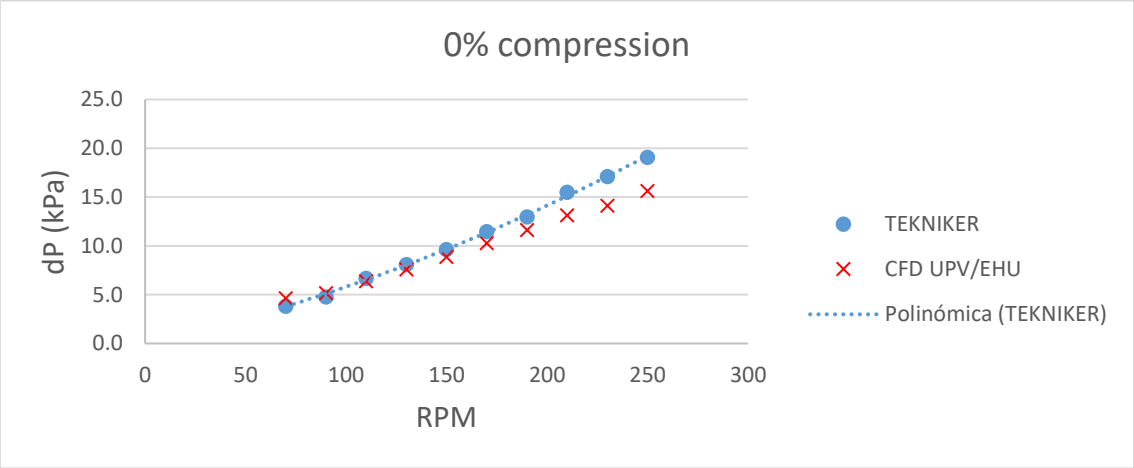

Figure 24. Model validation for 0% compression.

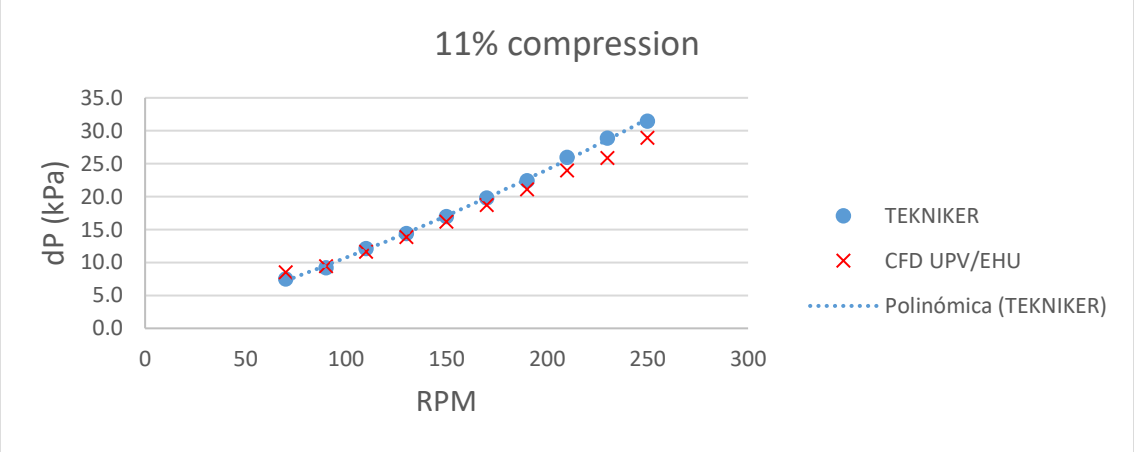

Figure 25. Model validation for 11% compression.

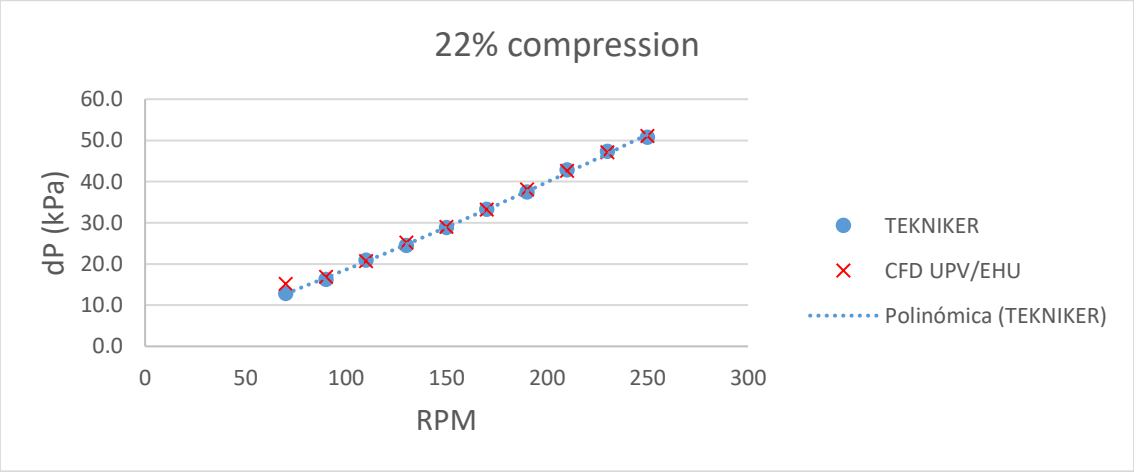

Figure 26. Model validation for 22% compression.

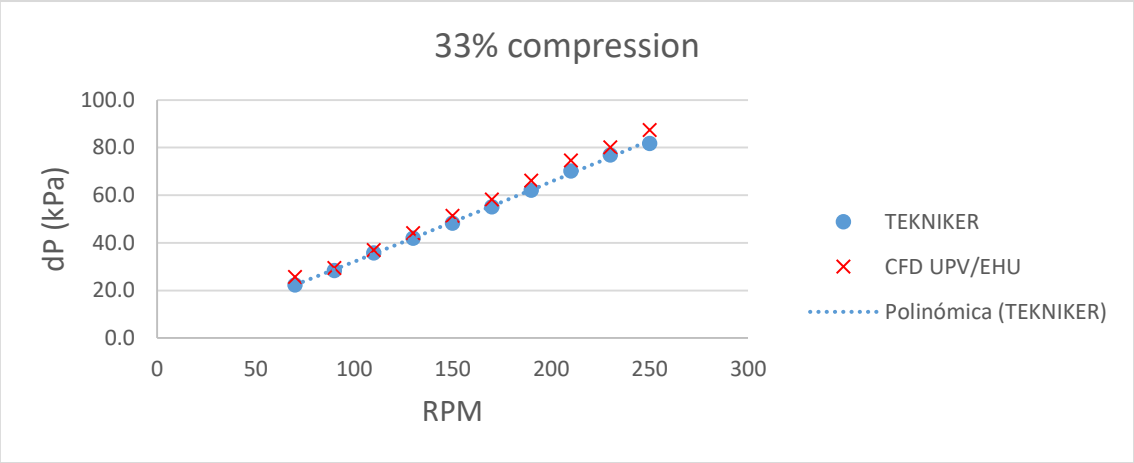

Figure 27. Model validation for 33% compression.

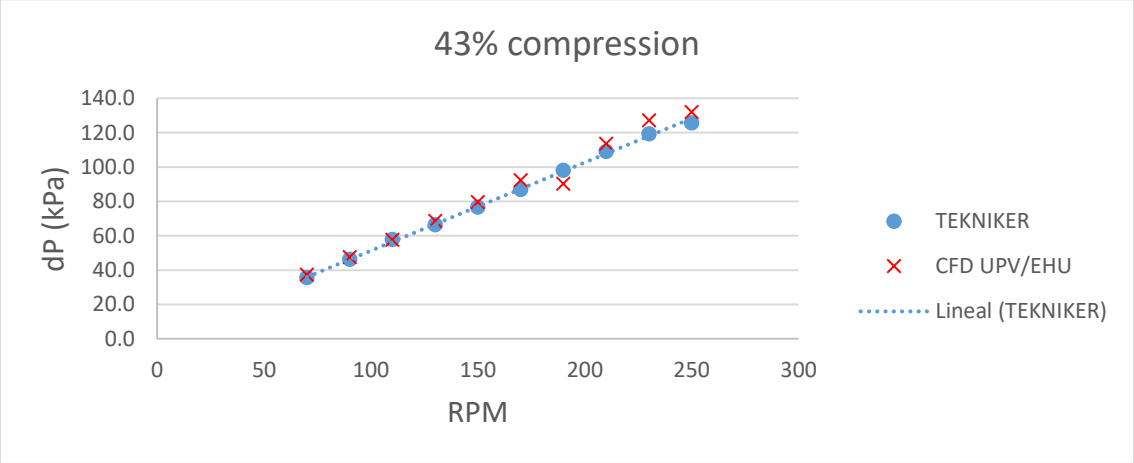

Figure 28. Model validation for 43% compression.

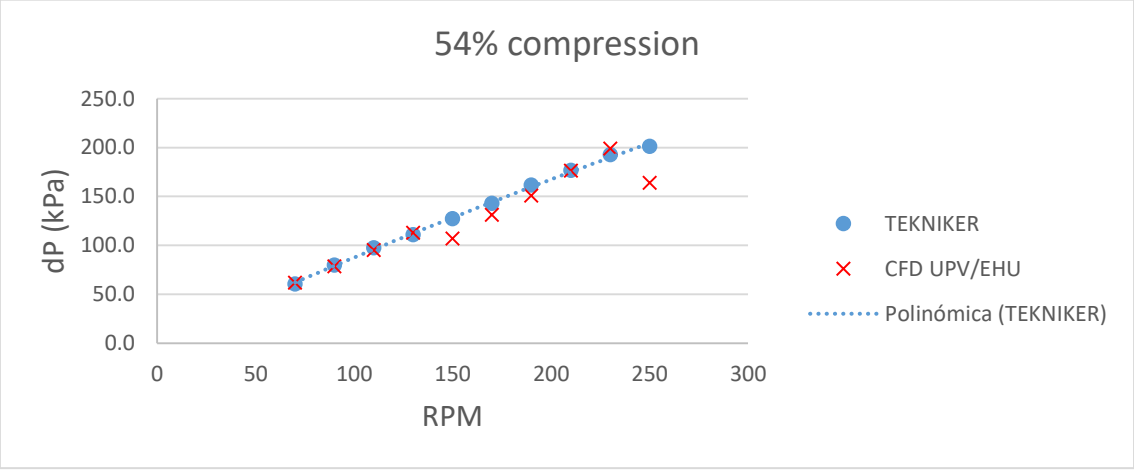

Figure 29. Model validation for 54% compression.

In order to analyse the influence of the electrode compression, the following graph shows the curves belonging to the six simulated compressions together. Note that this graphic shows pressure loss per unit of length instead of only pressure drop. In this way the influence of compression can be better appreciated. As the electrode compression increases, the pressure drop does the same. In fact, the higher the compression, the greater the influence on the pressure drop.

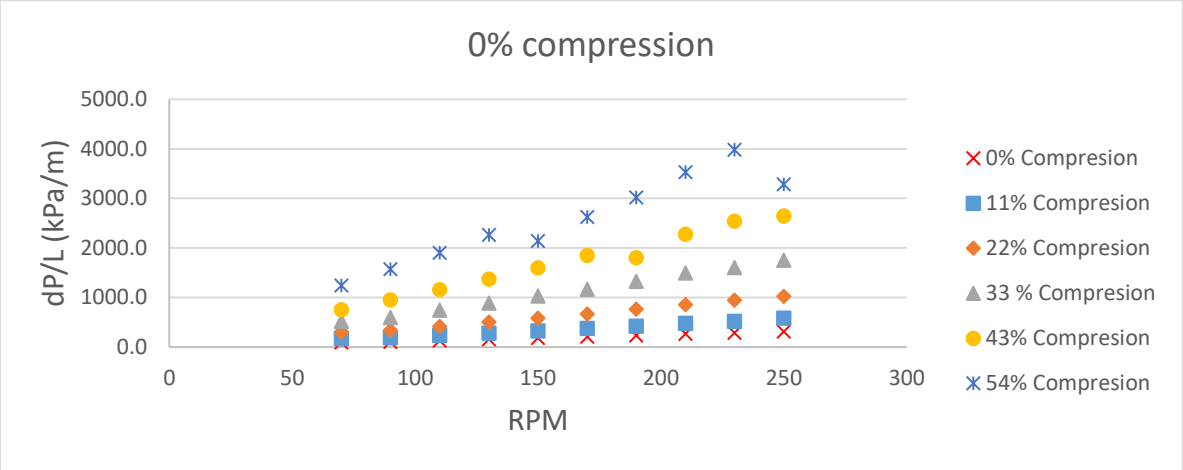

Figure 30. Influence of compression in pressure drop.

Figure 31 correspond to the cases of 0 and 22% compression respectively, at 250 RPM. Observing the scale of values of the pressure field, we confirm the tendency observed in Figure 30, that the higher the compression, the greater the pressure drop in the electrode.

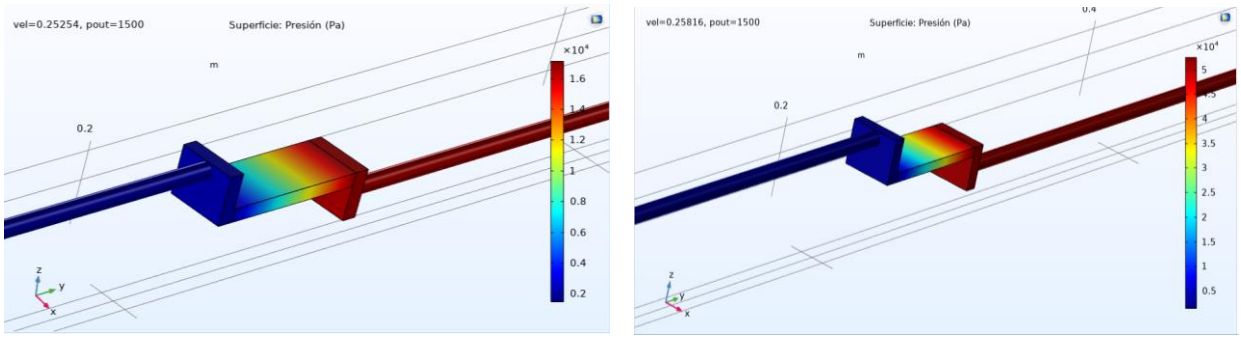

Figure 31. 0% compresion (left) and 22% compression (right).

3.2. PARAMETRIC STUDY-ELECTRODE DIMENSIONS

Once the model is validated and the effects of compression have been appreciated, a parametric study has been carried out. Starting from the geometry used above, two dimensions, A and B, will be modified, as shown in the following figure. Both dimensions are directly related to the physical dimensions of the electrode, so it will be possible to analyse the influence of the porous region on the fluid dynamics.

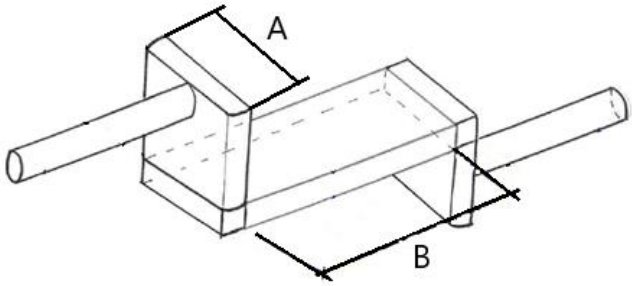

Figure 32. Sketch variation.

The tested measurements are shown in Table 8:

Table 8. Tested Measurements.

	A (mm)	B (mm)
Measurements 1	20	50
Measurements 2	31,62	31,62
Measurements 3	50	20

In order to clarify the scheme to be followed for the cases to be simulated, a tree diagram is shown below.

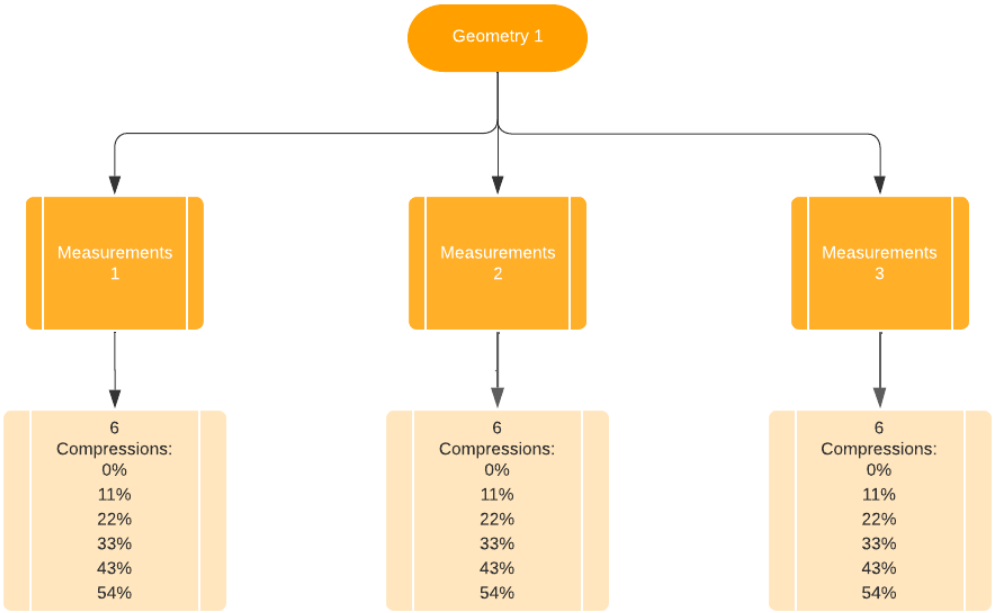

Figure 33. Simulation cases tree diagram.

3.2.1. RESULTS

The results obtained for the different electrode dimensions are shown below. M1 refers to Measurements 1, M2 to Measurements 2 and M3 to Measurements 3. In this way we can compare for each compression and RPM the influence it has on the pressure drop.

As it can be seen, the pressure drop is considerably reduced when going from Measurements 1 to Measurements 2. In fact, up to 60% less pressure drop is achieved. Looking at M3, the pressure drop continues to decrease. However, the variation from M2 to M3 is smaller than from M1 to M2.

This is mainly due to the distance the fluid has to travel in the porous region, i.e. how long our electrode is. In this case, that distance corresponds to dimension B in Figure 32. In Figures 40 and 41 pressure contours for M1, M2 and M3 at 0% compression and 250 RPM are shown. Looking at them, it is clear that a large part of the pressure loss occurs at the electrode, i.e. where the fluid encounters the greatest opposition to flow. This underlines the fact that the greater the distance the fluid has to travel in the porous medium, the greater the pressure loss in the battery. Furthermore, Figure 42, which represents the velocity field in the longitudinal plane, shows the decrease in the velocity of the electrolyte when reaching the electrode.

It should be mentioned that the lack of points in the cases of higher compressions is due to the lack of convergence in the simulations.

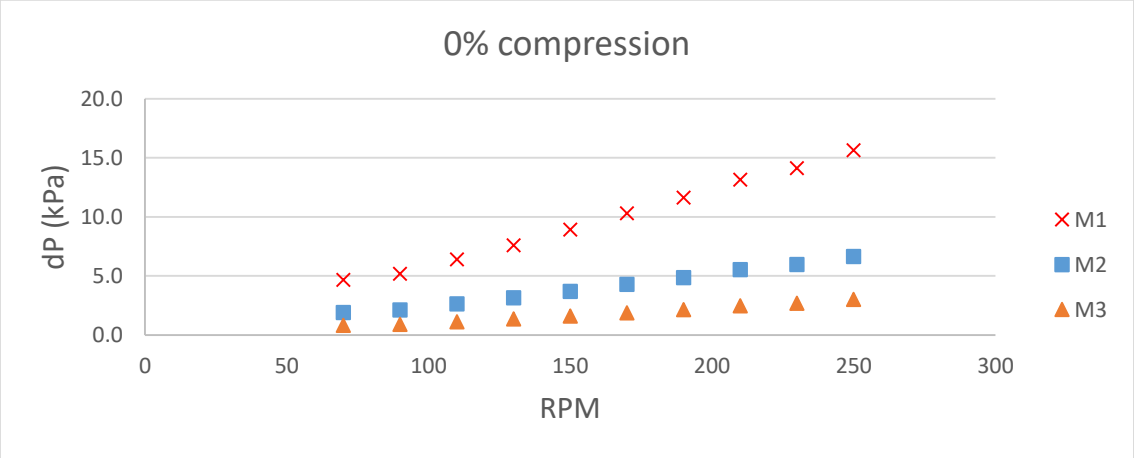

Figure 34. 0% compression for M1, M2 and M3.

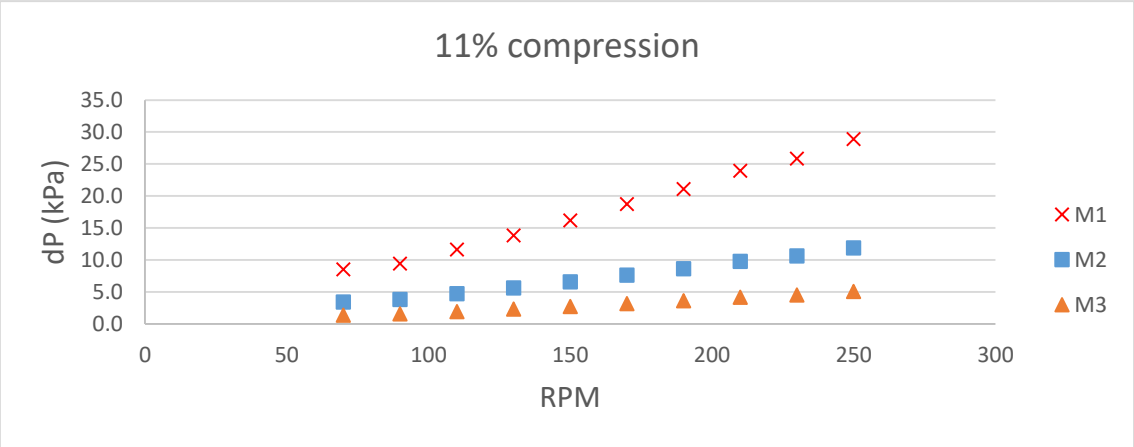

Figure 35. 11% compression for M1, M2 and M3.

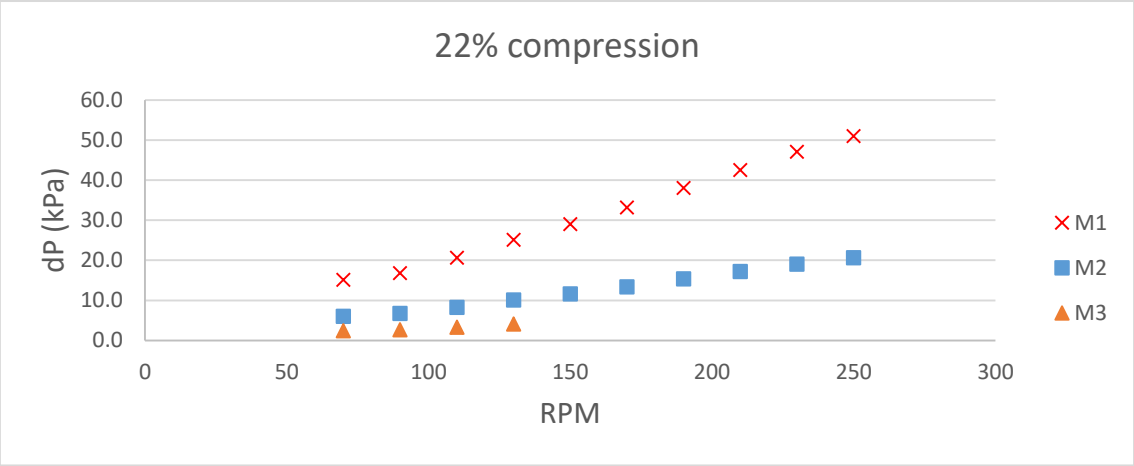

Figure 36. 22% compression for M1, M2 and M3.

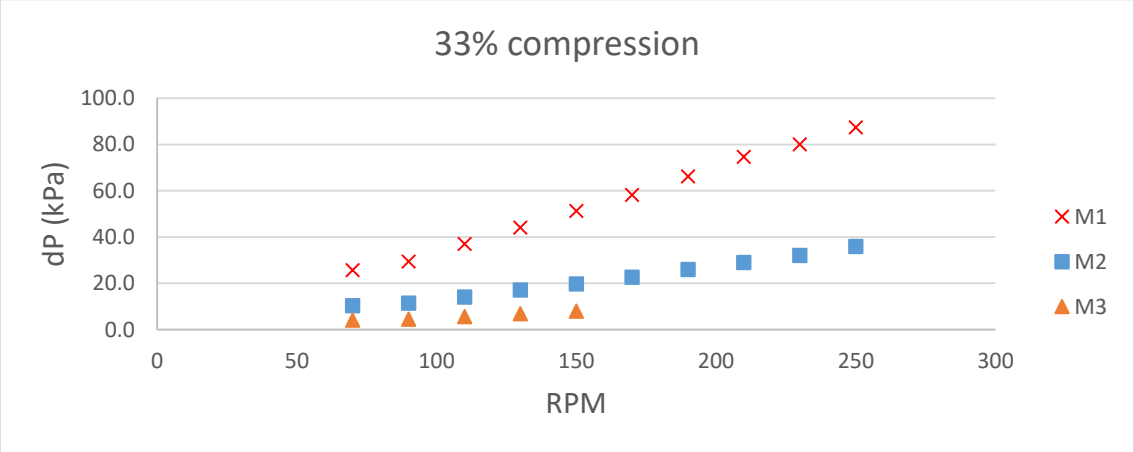

Figure 37. 33% compression for M1, M2 and M3.

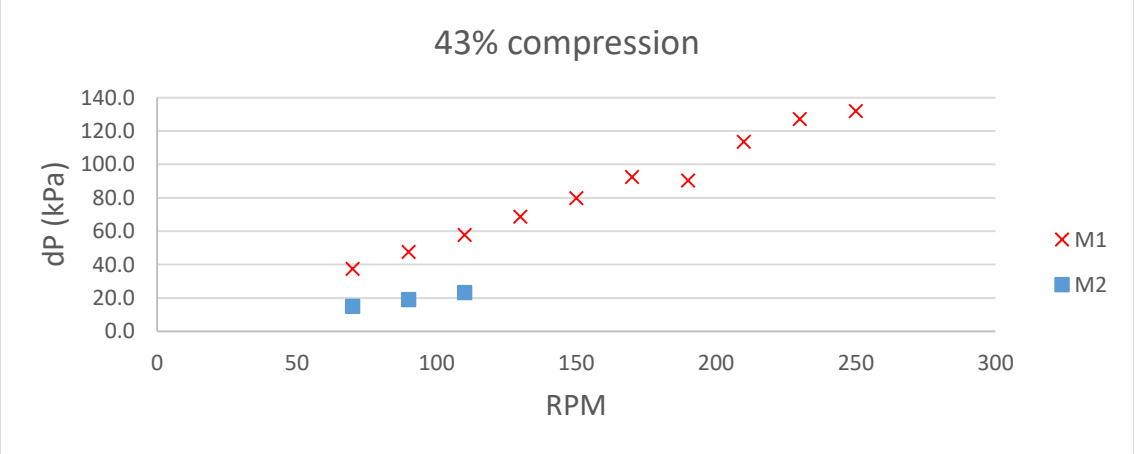

Figure 38. 43% compression for M1, M2 and M3.

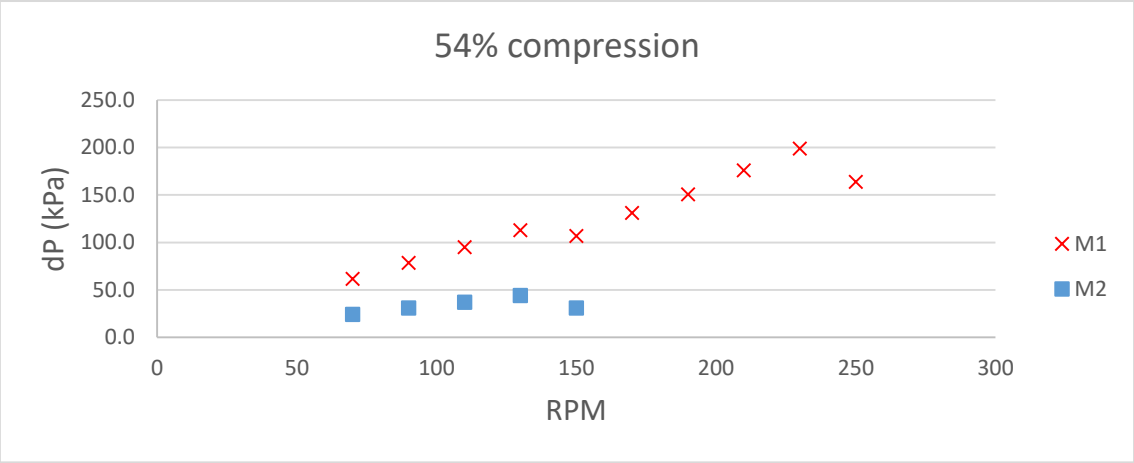

Figure 39. 54% compression for M1, M2 and M3.

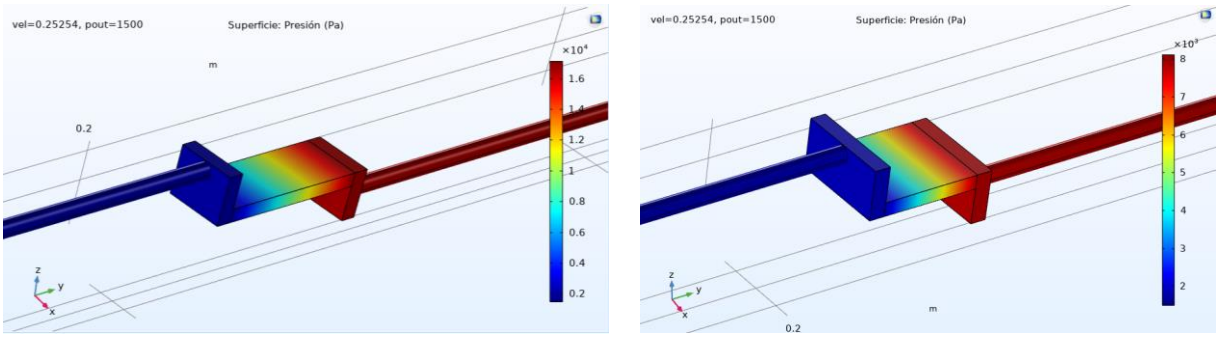

Figure 40. Pressure contours for M1 and M2 at 0% compression and 250 RPM.

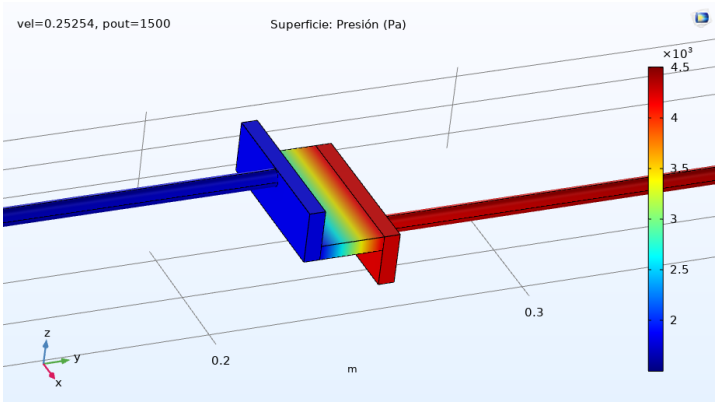

Figure 41. Pressure contour for M3 at 0% compression and 250 RPM.

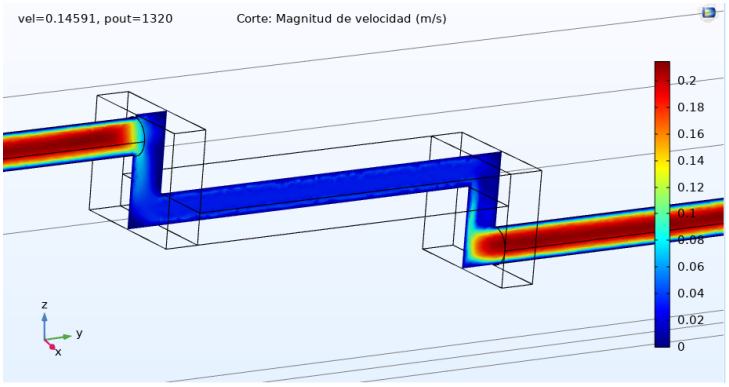

Figure 42. Velocity field in YZ plane at 0% compression.

3.3. PARAMETRIC STUDY-EXTERNAL GEOMETRY

The next step in the analysis is to vary the geometry of the battery itself. In other words, varying the geometry of the electrolyte inlets and outlets and their position relative to the electrode.

The two new proposals are shown in Figure 43 and 44 . In these cases the electrode is shown at the same height as the inlet and outlet, i.e. the electrolyte flow is not altered by changes in height. The first geometry discussed above will be referred to as G1, while the two new ones will be G2 and G3 respectively.

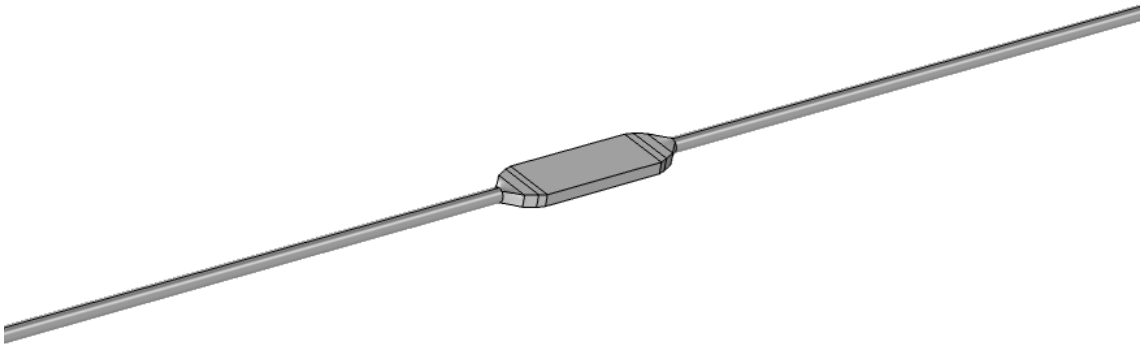

Figure 43. New geometry G2.

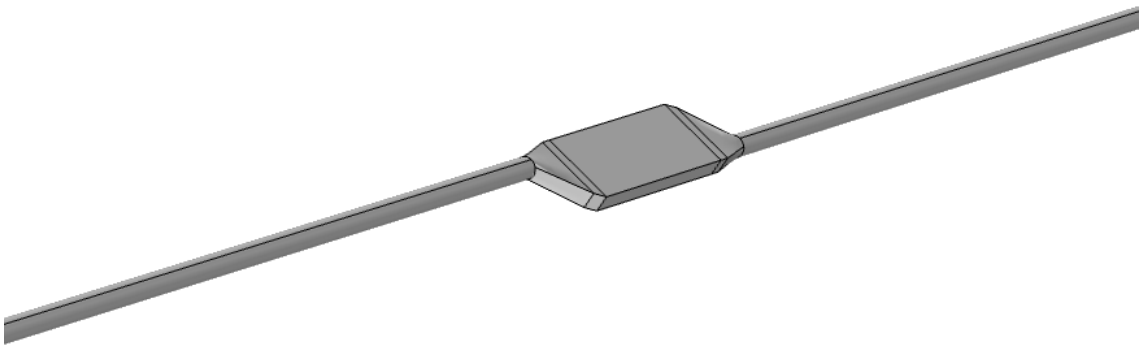

Figure 44. New geometry G3.

In addition, for each of these new models, the same study of the electrode dimensions will be carried out as for the first geometry. In this way, it will be possible to corroborate whether the previously observed trends are maintained.

3.3.1. RESULTS

The results obtained for geometries G2 and G3 show the same trends as G1 when varying the electrode dimensions. When going from M1 to M2 the reduction of the pressure drop is very noticeable, and when going to M3 it decreases again, although to a lesser extent. This confirms the fact that the most influential parameter is the length of the electrode, i.e. how far the electrolyte has to travel through the porous medium.

On the other hand, the higher the RPM, the higher the pressure drop. Similarly, when the electrode compression is increased, the pressure drop also increases.

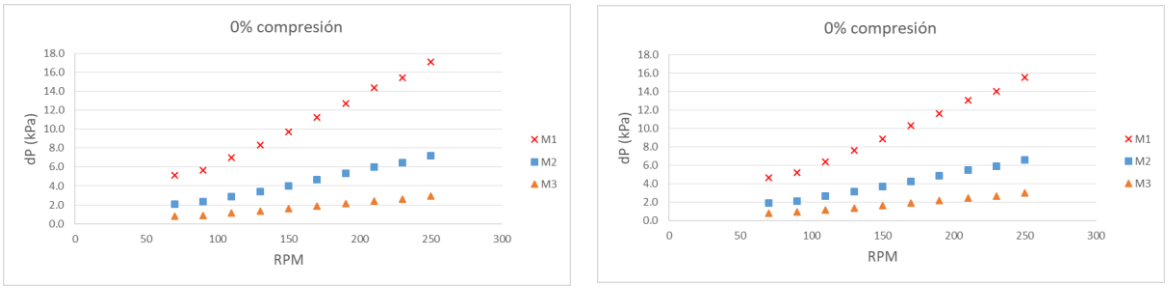

Figure 45. 0% compression for G2 (left) and G3 (right).

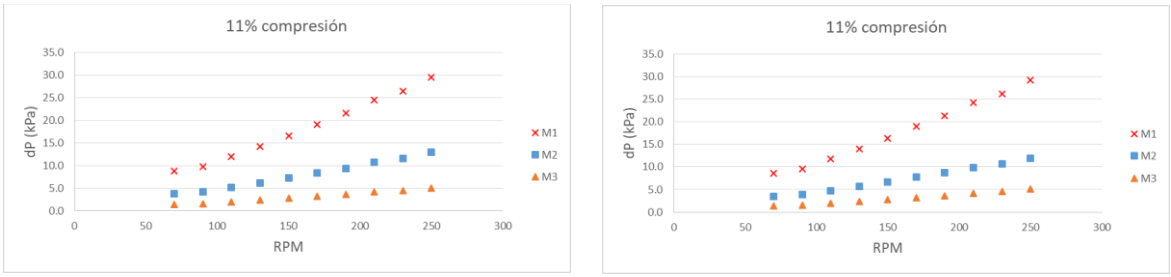

Figure 46. 11% compression for G2 (left) and G3 (right).

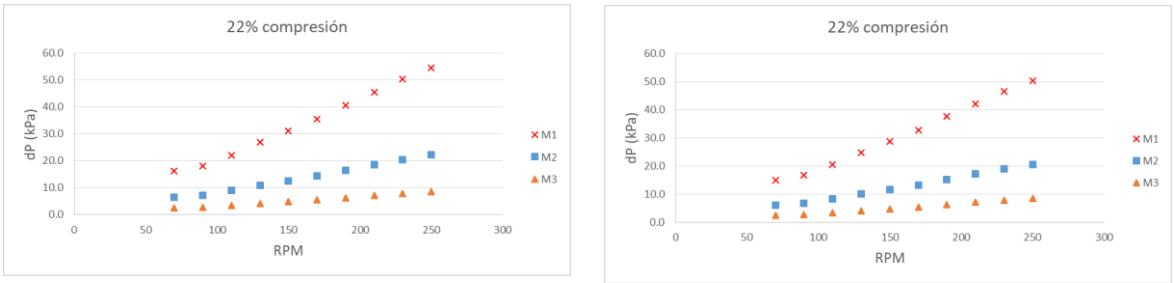

Figure 47. 22% compression for G2 (left) and G3 (right).

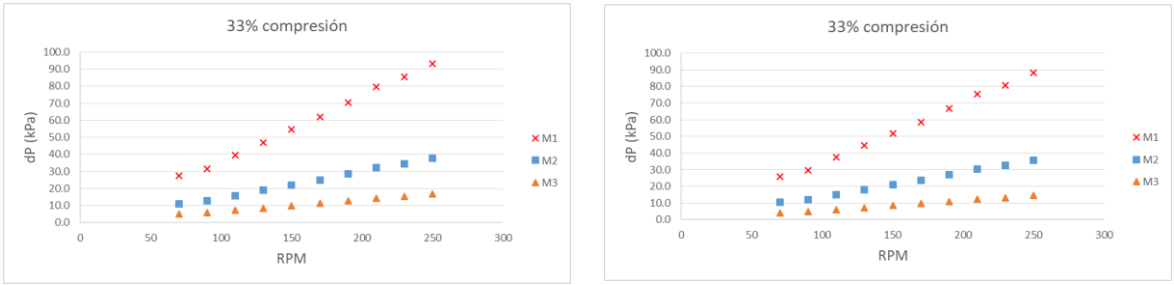

Figure 48. 33% compression for G2 (left) and G3 (right).

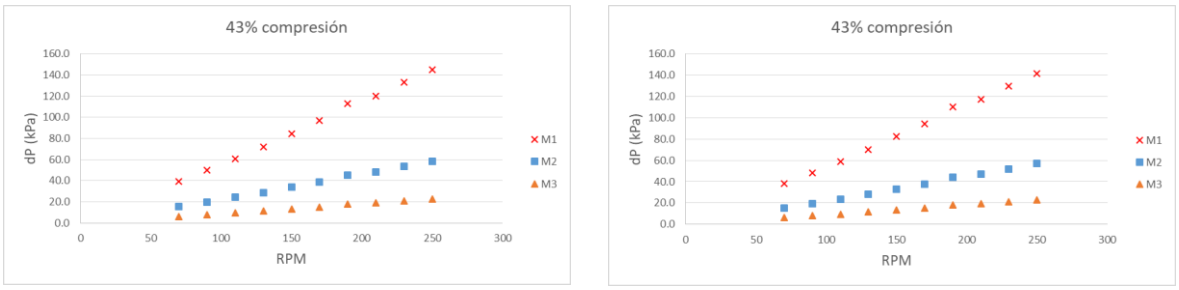

Figure 49. 43% compression for G2 (left) and G3 (right).

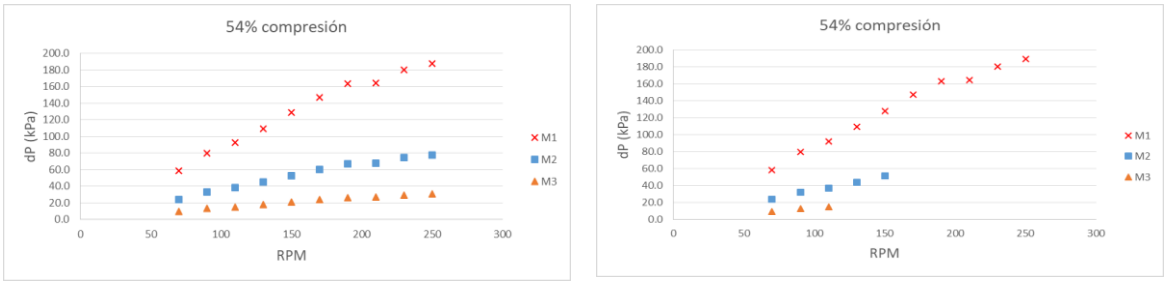

Figure 50. 54% compression for G2 (left) and G3 (right).

As observed in Figure 40 and 41, great part of the pressure loss happens in the electrode, shown in Figure 51. This observable trend helps to confirm the influence of the electrode dimensions in this study.

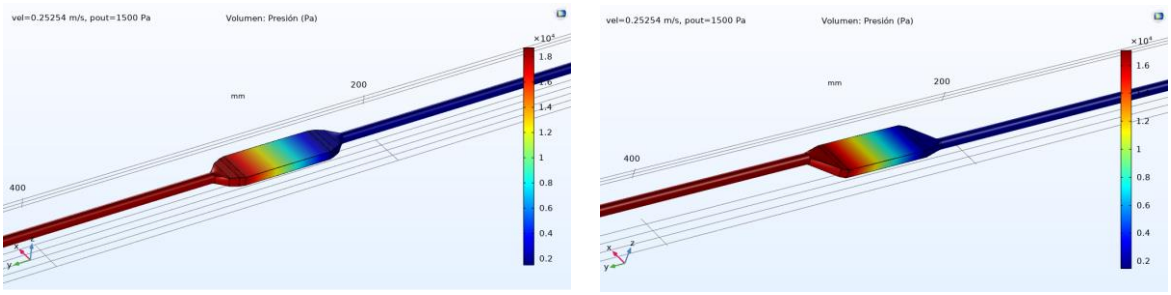

Figure 51. Pressure contours of G2 (left) and G3 (right) at 0% compression.

After the analysis of the influence of the electrode dimensions for the different geometries, the three geometries will be compared with each other. In this way, given the same electrode dimensions, the influence of the external geometry itself can be determined.

The graphs for G1, G2 and G3 for Measurements 1 are shown below. It is remarkable that for the 3 models, and in all cases of compression and RPM, the values obtained are practically the same. This shows that the shape of the external geometry, i.e. how the fluid inlets and outlets are positioned, has no significant impact on the pressure drop.

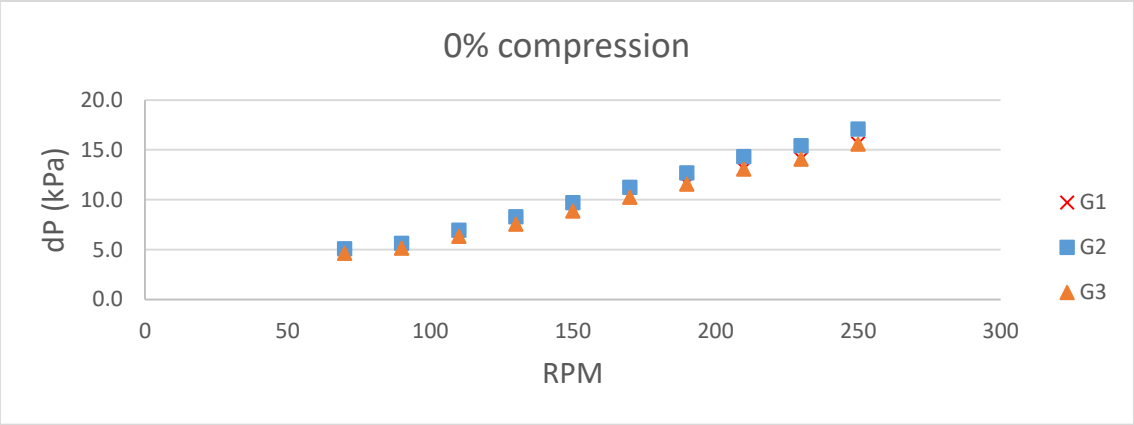

Figure 52. 0% compression for G1, G2 and G3.

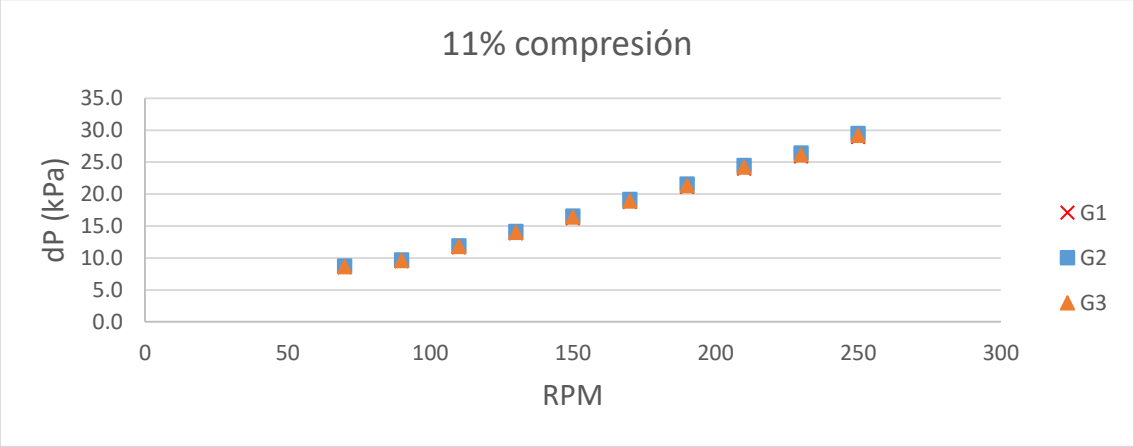

Figure 53. 11% compression for G1, G2 and G3.

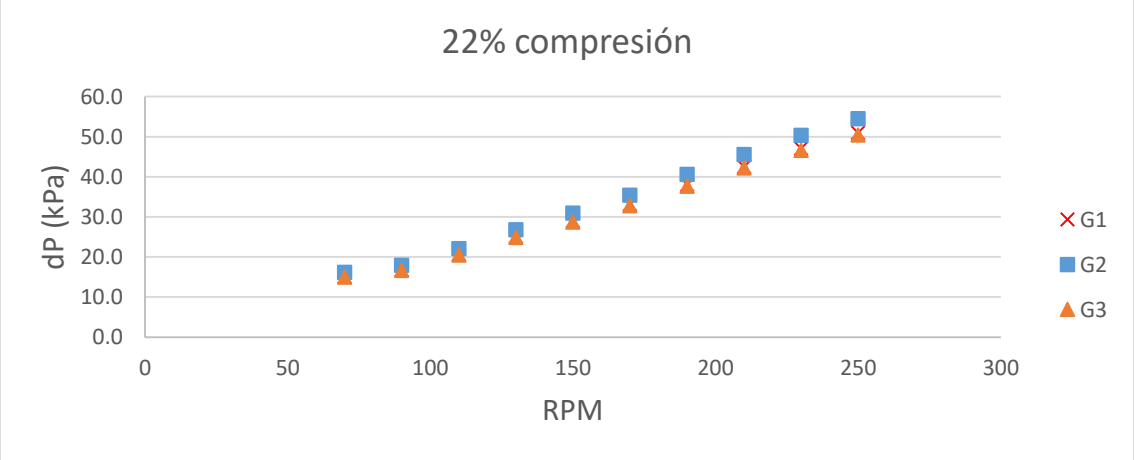

Figure 54. 22% compression for G1, G2 and G3.

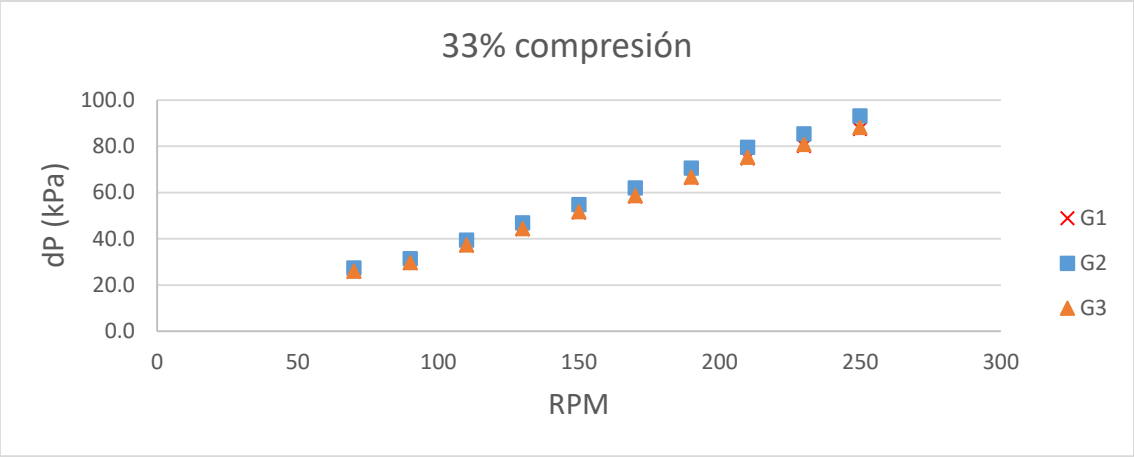

Figure 55. 33% compression for G1, G2 and G3.

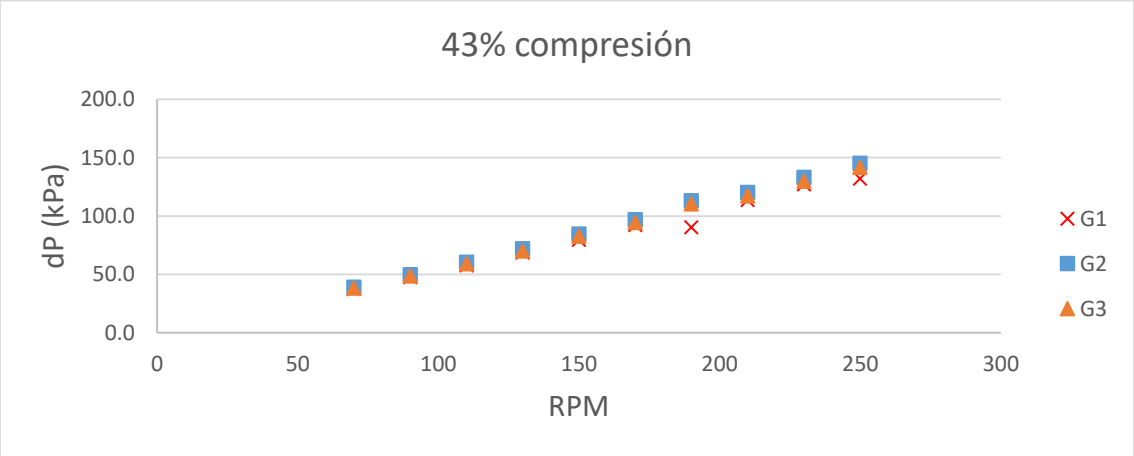

Figure 56. 43% compression for G1, G2 and G3.

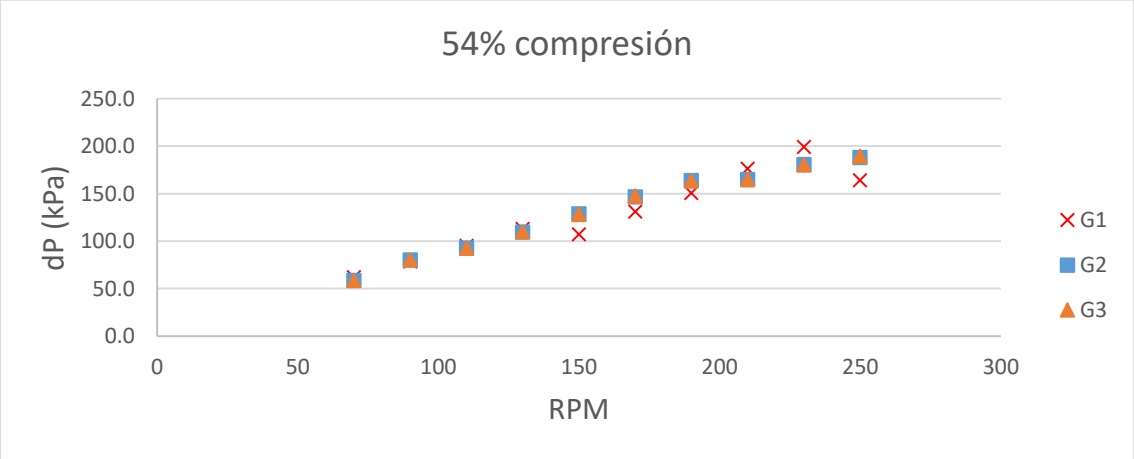

Figure 57. 54% compression for G1, G2 and G3.

4. PROJECT BUDGET

In this section a study is made on the budget necessary to carry out this project. Various concepts such as computer resources, both software and hardware, engineer labour and simulation cost are taken into account. For the engineer's labour a value of 150 €/hour is estimated. As for the cost of computer resources, a 16-core workstation valued at €2,000 has been used. A period of 4 years has been set for its amortisation.

As for the software, the COMSOL Multiphysics programme has been used to carry out the simulations, the licence for which is valued at €6,000. For the CAD design, the NX 12 Siemens software was used, which costs €24,000 per year to license. Both programs have been amortised over 1 year.

Table 9. Engineer labour costs.

Concept	Cost (€/h)	Quantity (h)	Total Cost (€)
Information search	150	50	7,500
CAD design	150	15	2,250
Simulation preparation	150	40	6,000
Results analysis	150	75	11,250
Documents drafting	150	100	15,000
	TOTAL (€)		**42,000**

Table 10. Amortisation.

Concept	Cost (€/h)	Quantity (h)	Total Cost (€)
Workstation	0.33	1,405	463.65
NX 12	16	15	240
COMSOL	4	1,125	4,500
	TOTAL (€)		**5,203.65**

Table 11. Total cost.

Concept	Total Cost (€)
Engineer labour cost	42,000
Amortisation	5,203.65
TOTAL (€)	**47,203.65**

5. CONCLUSIONS

After carrying out the numerical model and comparing its results with the experimental ones, a series of conclusions can be drawn:

- The numerical model developed using CFD techniques is valid and accurately reflects the results obtained experimentally.
- The impact of increasing the RPM of the pump is demonstrated, since it greatly increases the pressure loss.
- The compression of the electrode plays a fundamental role as we have already seen. The higher the compression, the greater the increase in pressure loss.
- Cases of higher compression are affected by convergence problems in the CFD. This is due to the gradients formed by compressing the electrode so much, which complicates the convergence of the solution.
- After performing the analysis by varying the electrode dimensions, it is shown that the length of the electrode is the most important parameter. Reducing the length has shown to have a significant impact on reducing the pressure drop.
- By means of pressure contours, it is visually confirmed that most of the pressure drop occurs in the area of the electrode.
- As seen in the analysis of the external geometry, the position of the electrolyte inlets and outlets shows no influence. In fact, the three geoemetries tested have practically the same results.

5.1. FUTURE WORKS

In order to continue this line of research, there are certain aspects that could be pursued in future work:

- Variable compression electrode: This consists of compressing the electrode progressively in the direction of flow. This could notably affect the fluid-dynamic aspects and even affect the electrochemistry itself.
- Cylindrical cell geometry: This arrangement could present different results by completely varying the structure of the geometry and the flow path itself.
- Electrochemistry: Apply these results to the electrochemistry of the complete battery to see what effect it has on the performance of the battery itself.
- Different electrodes: analyse the differences that different and newer types of electrodes can cause, either in terms of material, properties or microstructure.

6. BIBLIOGRAPHY

[1] A. M. Omer, «Energy, environment and sustainable development», *Renewable and Sustainable Energy Reviews*, vol. 12, n.º 9, pp. 2265-2300, dic. 2008, doi: 10.1016/j.rser.2007.05.001.

[2] M. Hafner y S. Tagliapietra, «The Global Energy Transition: A Review of the Existing Literature», en *The Geopolitics of the Global Energy Transition*, M. Hafner y S. Tagliapietra, Eds. Cham: Springer International Publishing, 2020, pp. 1-24. doi: 10.1007/978-3-030-39066-2_1.

[3] «Archive:Electricity generation statistics – first results - Statistics Explained». https://ec.europa.eu/eurostat/statistics-explained/index.php?title=Electricity_generation_statistics_%E2%80%93_first_results&oldid=498612#Production_of_electricity (accedido 2 de junio de 2022).

[4] P. A. Owusu y S. Asumadu-Sarkodie, «A review of renewable energy sources, sustainability issues and climate change mitigation», *Cogent Engineering*, vol. 3, n.º 1, p. 1167990, dic. 2016, doi: 10.1080/23311916.2016.1167990.

[5] E. Hossain, H. Faruque, Md. Sunny, N. Mohammad, y N. Nawar, «A Comprehensive Review on Energy Storage Systems: Types, Comparison, Current Scenario, Applications, Barriers, and Potential Solutions, Policies, and Future Prospects», *Energies*, vol. 13, n.º 14, p. 3651, jul. 2020, doi: 10.3390/en13143651.

[6] A. G. Olabi, C. Onumaegbu, T. Wilberforce, M. Ramadan, M. A. Abdelkareem, y A. H. Al – Alami, «Critical review of energy storage systems», *Energy*, vol. 214, p. 118987, ene. 2021, doi: 10.1016/j.energy.2020.118987.

[7] T. M. Gür, «Review of electrical energy storage technologies, materials and systems: challenges and prospects for large-scale grid storage», *Energy Environ. Sci.*, vol. 11, n.º 10, pp. 2696-2767, 2018, doi: 10.1039/C8EE01419A.

[8] «Benefits of Energy Storage | Energy Storage Assocation», *Energy Storage Association*. https://energystorage.org/why-energy-storage/benefits/ (accedido 6 de junio de 2022).

[9] «The Benefits of Energy Storage | EnergySage». https://www.energysage.com/energy-storage/benefits-of-storage/ (accedido 6 de junio de 2022).

[10] «Five Benefits of Energy Storage: The Holy Grail of Energy», *Facilitiesnet*. https://www.facilitiesnet.com/energyefficiency/article/Five-Benefits-of-Energy-Storage-The-Holy-Grail-of-Energy--16907 (accedido 6 de junio de 2022).

[11] «The Benefits of Energy Storage for Commercial and Industrial Facilities», *Dynapower*, 12 de julio de 2019. https://dynapower.com/benefits-of-energy-storage/ (accedido 6 de junio de 2022).

[12] E. Sum y M. Skyllas-Kazacos, «A study of the V(II)/V(III) redox couple for redox flow cell applications», *Journal of Power Sources*, vol. 15, n.º 2, pp. 179-190, jun. 1985, doi: 10.1016/0378-7753(85)80071-9.

[13] M. Messaggi *et al.*, «Analysis of flow field design on vanadium redox flow battery performance: Development of 3D computational fluid dynamic model and experimental validation», *Applied Energy*, vol. 228, pp. 1057-1070, oct. 2018, doi: 10.1016/j.apenergy.2018.06.148.

[14] M. Dassisti *et al.*, «Vanadium: A Transition Metal for Sustainable Energy Storing in Redox Flow Batteries», en *Reference Module in Materials Science and Materials Engineering*, Elsevier, 2016, p. B9780128035818040000. doi: 10.1016/B978-0-12-803581-8.04007-8.

[15] N. Zimmerman, «VANADIUM REDOX FLOW BATTERY», p. 68.

[16] «VRFB components». http://www.h2aec.com/eng/sub/tech/tech.php (accedido 6 de junio de 2022).

[17] X. Yuan *et al.*, «A review of all-vanadium redox flow battery durability: Degradation mechanisms and mitigation strategies», *Int J Energy Res*, p. er.4607, jun. 2019, doi: 10.1002/er.4607.

[18] K. Lourenssen, J. Williams, F. Ahmadpour, R. Clemmer, y S. Tasnim, «Vanadium redox flow batteries: A comprehensive review», *Journal of Energy Storage*, vol. 25, p. 100844, oct. 2019, doi: 10.1016/j.est.2019.100844.

[19] K. J. Kim, M.-S. Park, Y.-J. Kim, J. H. Kim, S. X. Dou, y M. Skyllas-Kazacos, «A technology review of electrodes and reaction mechanisms in vanadium redox flow batteries», *J. Mater. Chem. A*, vol. 3, n.º 33, pp. 16913-16933, ago. 2015, doi: 10.1039/C5TA02613J.

[20] D. S. Aaron *et al.*, «Dramatic performance gains in vanadium redox flow batteries through modified cell architecture», *Journal of Power Sources*, vol. 206, pp. 450-453, may 2012, doi: 10.1016/j.jpowsour.2011.12.026.

[21] P. K. Leung, M. R. Mohamed, A. A. Shah, Q. Xu, y M. B. Conde-Duran, «A mixed acid based vanadium–cerium redox flow battery with a zero-gap serpentine architecture», *Journal of Power Sources*, vol. 274, pp. 651-658, ene. 2015, doi: 10.1016/j.jpowsour.2014.10.034.

[22] I. Aramendia, U. Fernandez-Gamiz, A. Martinez-San-Vicente, E. Zulueta, y J. M. Lopez-Guede, «Vanadium Redox Flow Batteries: A Review Oriented to Fluid-Dynamic Optimization», *Energies*, vol. 14, n.º 1, p. 176, dic. 2020, doi: 10.3390/en14010176.

[23] J. A. Trainham y J. Newman, «A comparison between flow-through and flow-by porous electrodes for redox energy storage», *Electrochimica Acta*, vol. 26, n.º 4, pp. 455-469, abr. 1981, doi: 10.1016/0013-4686(81)87024-7.

[24] Q. Xu, T. S. Zhao, y P. K. Leung, «Numerical investigations of flow field designs for vanadium redox flow batteries», *Applied Energy*, vol. 105, pp. 47-56, may 2013, doi: 10.1016/j.apenergy.2012.12.041.

[25] J. D. Anderson, *Computational fluid dynamics: the basics with applications*. New York: McGraw-Hill, 1995.

[26] A. Atangana, «Chapter 2 - Principle of Groundwater Flow», en *Fractional Operators with Constant and Variable Order with Application to Geo-Hydrology*, A. Atangana, Ed. Academic Press, 2018, pp. 15-47. doi: 10.1016/B978-0-12-809670-3.00002-3.

[27] «2.5: Darcy's Law - Flow in a Porous Medium - Geosciences LibreTexts». https://geo.libretexts.org/Courses/University_of_California_Davis/GEL_056%3A_Introduction_to_Geophysics/Geophysics_is_everywhere_in_geology.../02%3A_Diffusion_and_Darcy's_Law/2.05%3A_Darcy's_Law_-_Flow_in_a_Porous_Medium (accedido 6 de junio de 2022).

[28] X. Ke, J. Prahl, J. Alexander, y R. Savinell, «Redox flow batteries with serpentine flow fields: Distributions of electrolyte flow reactant penetration into the porous carbon electrodes and effects on performance», *Journal of Power Sources*, vol. 384, pp. 295-302, mar. 2018, doi: 10.1016/j.jpowsour.2018.03.001.

[29] SGL Group, «Specialty Graphites for Energy Storage».

[30] «Introduction to the Porous Media Flow Module», p. 38.